KfK 4899
November 1991

Neutron Capture in $^{122, 123, 124}$Te: A Critical Test for s-Process Studies

K. Wisshak, F. Voß, F. Käppeler, G. Reffo
Institut für Kernphysik

Kernforschungszentrum Karlsruhe

KERNFORSCHUNGSZENTRUM KARLSRUHE

Institut für Kernphysik

KfK 4899

NEUTRON CAPTURE IN ^{122,123,124}Te: A CRITICAL TEST FOR s-PROCESS STUDIES.

K. Wisshak, F. Voß, F. Käppeler, and G. Reffo*

*Permanent address: E.N.E.A. Bologna, Viale Ercolani 8, I-40138 Bologna, Italy

Kernforschungszentrum Karlsruhe GmbH, Karlsruhe

Kernforschungszentrum Karlsruhe GmbH
Postfach 3640, 7500 Karlsruhe 1

ISSN 0303-4003

ABSTRACT

The neutron capture cross sections of ^{122,123,124,125,126}Te were measured in the energy range from 10 to 200 keV at the Karlsruhe Van de Graaff accelerator using gold as a standard. Neutrons were produced via the ^{7}Li(p,n)^{7}Be reaction by bombarding metallic Li targets with a pulsed proton beam. Capture events were registered with the Karlsruhe 4π Barium Fluoride Detector. Several runs have been performed under different experimental conditions to study the systematic uncertainties in detail. The cross section ratios were determined with an overall uncertainty of ~1 %. This is an improvement by about a factor of five compared to the existing data.

Maxwellian averaged neutron capture cross sections were calculated for thermal energies between kT = 10 and 100 keV by normalizing the cross section shape up to 600 keV neutron energy reported in literature to the present data. These stellar cross sections were used in an s-process analysis. With the classical approach the abundances of the three s-only isotopes ^{122,123,124}Te could be reproduced within the experimental uncertainties of ~1 %. The accuracy of the present data allowed also to derive constraints for the existing stellar models with respect to the effective neutron density. Furthermore, the p-process abundances for the tellurium isotopes are discussed.

ZUSAMMENFASSUNG

NEUTRONENEINFANG IN ^{122,123,124}Te: EIN EMPFINDLICHER TEST FÜR UNTERSUCHUNGEN ZUM s-PROZESS

Die Neutroneneinfangquerschnitte von ^{122,123,124,125,126}Te wurden im Energiebereich von 10 bis 200 keV am Karlsruher Van de Graaff Beschleuniger relativ zu Gold als Standard bestimmt. Neutronen wurden über die ^{7}Li(p,n)^{7}Be Reaktion durch Beschuß metallischer Li Targets mit einem gepulsten Protonenstrahl erzeugt. Einfangereignisse wurden mit dem Karlsruher 4π Barium Fluorid Detektor nachgewiesen. Daten wurden unter verschiedenen experimentellen Bedingungen aufgenommen, um die systematischen Unsicherheiten im einzelnen zu untersuchen. Die Verhältnisse der Wirkungsquerschnitte wurden mit einer Genauigkeit von ~1 % bestimmt. Dies bedeutet eine Verbesserung um einen Faktor fünf im Vergleich zu den existierenden Daten.

Über eine Maxwell Verteilung gemittelte Einfangquerschnitte wurden im Bereich von kT=10 bis 100 keV berechnet. Dazu wurde der Verlauf des Wirkungsquerschnittes bis 600 keV Neutronenenergie, der aus der Literatur bekannt ist, auf die vorliegenden Daten normiert. Diese stellaren Einfangquerschnitte wurden in einer Untersuchung des s-Prozesses verwendet. Mit der klassischen Methode wurden die Häufigkeiten der drei reinen s-Kerne ^{122,123,124}Te mit der experimentellen Unsicherheit von ~1 % reproduziert. Die Genauigkeit der vorliegenden Daten erlaubte weiterhin Sternmodelle bezüglich der effektiven Neutronendichte einzuschränken. Außerdem werden die p-Prozess Häufigkeiten der Tellur Isotope diskutiert.

CONTENTS

I. INTRODUCTION

The nucleosynthesis of the heavy elements by successive neutron captures in the so called s-process (s=slow neutron capture) is one of the topics in nuclear astrophysics that can be addressed in detail by laboratory experiments. The most important quantities in these investigations are the isotopic abundances, N_s , and the stellar neutron capture cross sections, $\langle\sigma\rangle$, averaged over a Maxwellian velocity distribution for a typical s-process temperature of $\sim 3 \cdot 10^8$ K corresponding to thermal energies around kT=30 keV. Model descriptions [1] showed that the product $N_s\langle\sigma\rangle$ is a smooth function of mass number A .

Most important for characterizing the $N_s\langle\sigma\rangle(A)$ - curve are those isotopes that are only produced in the s-process, since they are shielded from the r-process (r = rapid neutron capture) by stable isobars. In these cases, the s-process abundances, N_s, are identical with the solar abundances, $N_\odot$ (apart from minor p-process contributions , see section VII). The solar abundances are derived from the composition of primitive meteorites[2] and from the solar spectrum[3]. In certain mass regions it is possible to determine elemental abundance ratios with an uncertainty of ~2 % (Refs. 4,5) . Of special interest in s-process studies are those eight elements (Kr, Sr, Te, Xe, Ba, Sm, Gd, Os) with two or three s-only isotopes, since the abundance ratios of these isotopes are simply the isotopic ratios that are known with typical uncertainties of 0.1 % (Ref. 6). Therefore, these examples represent the most sensitive probes for details of the s-process environment.

Informations on the physical conditions during the s-process, e.g. neutron density, temperature, and electron density can be deduced from the analysis of branchings in the s-process path[1]. The branchings result from the competition between neutron capture and beta decay whenever an unstable isotope is encountered by the s-process path, that exhibits a beta decay rate, $\lambda_\beta = \ln 2 / t_{1/2}$, comparable to its neutron capture rate, $\lambda_n = n_n v_T \langle\sigma\rangle$. In these expressions, $t_{1/2}$ is the half-life, n_n the s-process neutron density, v_T the mean thermal neutron velocity, and $\langle\sigma\rangle$ the stellar neutron capture cross section. The competition between beta decay and neutron capture defines the branching factor $f_n = \lambda_n/(\lambda_n+\lambda_\beta)$ for the s-process flow, which depends on the neutron density, n_n, and sometimes on temperature, T, since the half- life for beta decay may be temperature - dependent under stellar conditions. Stringent constraints on these parameters can be obtained from branchings that are defined by two s-only isotopes of the same element. The six branchings of this type are compiled in Table I, and are illustrated in Figure 1 by the example of the tellurium isotopes.

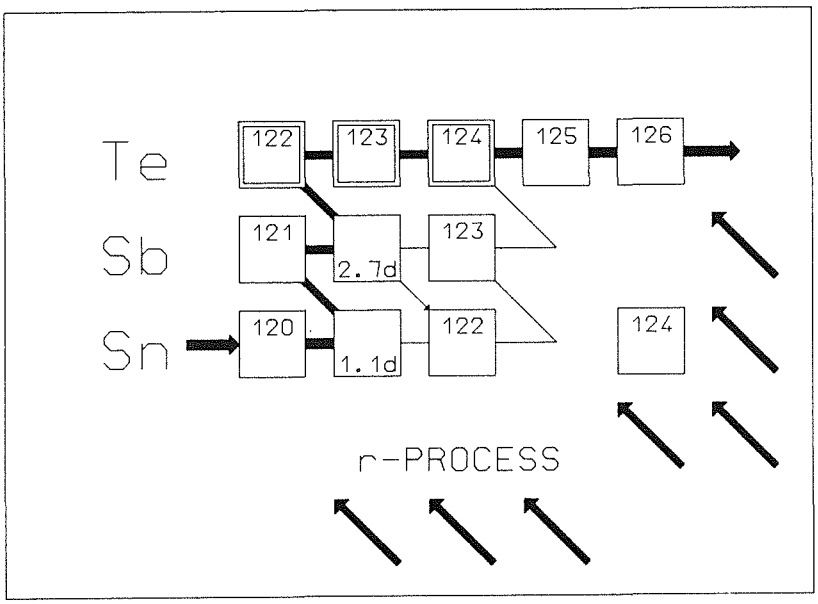

Fig. 1 The s-process path in the region of the tellurium isotopes. The s-only isotopes ^{122,123,124}Te are shielded from the r-process by the stable isobars ^{122,124}Sn and ^{123}Sb. The unstable nuclèi ^{121}Sn and ^{122}Sb are possible branching points.

TABLE I. Branchings in the s-process path with two s-only isotopes, which can be significantly improved by accurate cross section ratios.

s-only isotopes	branching point	branching factor f_n	sensitive physical parameter
^{80,82}Kr	^{79}Se	0.50±0.12	temperature
^{122,123,124}Te	^{121}Sn,^{122}Sb	0.01±0.05 *	neutron density
^{128,130}Xe	^{127}Te,^{128}I	0.01±0.25 *	electron density, xenon abundance
^{134,136}Ba	^{133}Xe,^{134}Cs	0.02±0.15 *	temperature and neutron density
^{148,150}Sm	^{147}Nd,^{147}Pm,^{148}Pm	0.10±0.05	neutron density
^{152,154}Gd	^{151}Sm,^{152}Eu	0.95±0.05	electron density

* estimates from classical model much smaller than current experimental uncertainty

Branchings at ^{121}Sn and ^{122}Sb cause part of the s-process flow to bypass ^{122}Te and ^{123}Te. In first approximation, the effect of these branchings is expressed by:

$$1-f_n \cong N_s\langle\sigma\rangle(^{122}\mathrm{Te})/N_s\langle\sigma\rangle(^{124}\mathrm{Te}) .$$

The uncertainty of this ratio is completely determined by the uncertainty of the cross sections. In a recent measurement by Macklin and Winters[7], an uncertainty of ±5 % was obtained. Since f_n is expected to range between 0.01 and 0.05 according to estimates with the classical approach and by stellar models, a considerable improvement of the cross sections is required for a quantitative analysis of these branchings.

A similar example is the branching at A = 147, 148, which is defined by the two s-only isotopes ^{148}Sm and ^{150}Sm . This case is most suited for the determination of the neutron density, n_n. In a careful experiment[8] using a conventional technique the cross section ratio was also determined with an uncertainty of ~4 %. In the branching analysis, this uncertainty represents the dominant contribution to the ± 40 % uncertainty of the deduced neutron density. Hence, a significant improvement can be expected from more accurate cross sections also for this branching.

The aim of the present experiment is to apply a new method , which allows to determine cross section ratios with an uncertainty of ~1 %. With such data on hand, it will be possible to improve our knowledge on the $N_s\langle\sigma\rangle(A)$-curve, and to check on the one percent level the prediction of the classical s-process model of a "local approximation", i.e. that the product $N_s\langle\sigma\rangle$ is constant for neighboring isotopes. Moreover, these data are the prerequisite for detailed analyses of the branchings listed in Table I, which will lead to significantly improved parameters for the physical conditions during the s-process. This information will then allow to improve the constraints for stellar models.

The most interesting candidates to start with are the isotopes of tellurium. Tellurium is the only element in nature with three s-only isotopes (see Fig. 1). From the classical model a very weak branching is predicted. Therefore it is the only possibility to check the local approximation for a chain of three neighboring isotopes. The unique fact that one of the s-only isotopes has an odd mass number and thus is not produced by the p-process (see Sec. VII) even allows to exclude the possibility that a weak branching is masked by a corresponding p-process contribution, an ambiguity that has to be discussed for all other branchings. In addition, the data are expected to yield an upper limit for the neutron

density as a constraint for current stellar models, and to allow for an estimate of the p-process contribution to the even tellurium isotopes.

In the following, we describe the experiment and data evaluation in Secs. II and III. The differential cross sections are presented in Sec. IV, while the uncertainties are discussed in Sec. V. Section VI is devoted to the determination of stellar cross sections, and the implications for the classical s-process approach are given in Sec. VII. A detailed discussion of the consequences for current stellar models will be the topic of a forthcoming publication.

II. EXPERIMENT

A. EXPERIMENTAL METHOD

The neutron capture cross sections of the tellurium isotopes 122 to 126 were measured in the energy range from 10 to 200 keV using gold as a standard. The experimental method has been published in detail in Refs. 9 and 10. Here only the most essential features are repeated and changes or improvements that were introduced since our first measurement on Nb, Ta, and Rh are described. Neutrons were produced via the $^{7}Li(p,n)^{7}Be$ reaction by bombarding metallic Li targets with the pulsed proton beam of the Karlsruhe 3.75 MV Van de Graaff accelerator. The neutron energy is determined by time of flight (TOF), the samples being located at a flight path of 78 cm. The important parameters of the accelerator are: pulse width ~1 ns, repetition rate 250 kHz, and average beam current 1.5 - 2 μA.

The neutron beam was collimated to 25 mm diameter at the sample position. The neutron flight path through collimator and detector was evacuated in order to eliminate background from neutrons scattered in the air. Since rather small sample masses are used in the present experiment, the scattering background due to the 50 cm flight path through the detector (see below) were otherwise compatible with the scattering effect of the samples. Two thin stainless steel tubes closed by 20 μm thick kapton foils were installed along the flight path leaving only a gap of ~1 cm for the samples . The central part of the collimator was evacuated, too.

In three different runs, the energy of the proton beam was adjusted 10, 30 and 100 keV above the reaction threshold of the $^{7}Li(p,n)^{7}Be$ reaction at 1.881 MeV. This yields continuous

neutron spectra in the energy range of interest for s-process studies, i.e. 10 - 70 keV, 3 - 100 keV, and 3 - 200 keV, respectively. The use of different spectra allowed to optimize the signal to background ratio in different neutron energy regions (see Sec. III). The thickness of the metallic lithium targets was chosen as to reduce the energy of the proton beam below the threshold of the (p,n)-reaction in order to minimize the intensity of gamma-rays produced by inelastic scattering (E_γ = 478 keV) on ^{7}Li, and by the ^{7}Li(p,γ) reaction (E_γ = 16 and 19 MeV). For the maximum energy loss of 100 keV a lithium layer of ~1mg/cm^2 was sufficient.

The Karlsruhe 4π Barium Fluoride Detector was used for the registration of capture gamma-ray cascades. This detector (a comprehensive description is given in Ref. 9) consists of 42 hexagonal and pentagonal crystals forming a spherical shell of BaF_2 with 10 cm inner radius and 15 cm thickness. It is characterized by a resolution in gamma-ray energy of 7 % at 2.5 MeV, a time resolution of 500 ps, and a peak efficiency of 90 % at 1 MeV. Capture events are registered with ~95 % probability.

The main advantages of this experimental method are the following: The entire capture cascade is detected with good energy resolution. Thus, ambiguities in the detection efficiency due to different cascade multiplicitys are avoided, and neutron capture events can be separated from gamma-ray background and background due to capture of sample scattered neutrons by selecting events with appropriate sum energy. The high granularity of the detector allows for a further separation of capture events and background by the event multiplicity . The short primary flight path and the inner radius of the detector guarantees that part of the TOF spectra is completely undisturbed by background from sample scattered neutrons (see Sec. III). This range with optimum signal to background ratio can be used to normalize the cross section. The high detection efficiency allows the use of small samples avoiding large multiple scattering corrections. Finally, the ^{7}Li(p,n)-reaction yields neutrons exactly and exclusively in the range of interest for s-process studies.

B. SAMPLES

Metallic, isotopically enriched samples have been used. The relevant parameters of the eight samples mounted simultaneously in the sample changer are compiled in Table II. The tellurium samples were pellets pressed from metal powder. Their weight was selected according to the expected cross sections in order to obtain similar capture yields per

TABLE II. Compilation of relevant sample data.

Sample[a]	Thickness [mm]	Thickness[b] [10^{-3} A/barn]	Weight [g]	Oxygen content [%][c]	Impurity[d] [%][c]	Neutron binding energy [MeV]
1.) Au	0.8	4.3427	1.11556	0	<0.01	6.513
2.) Graphite	1.3	10.579	0.16572	0		
3.) ^{122}Te	2.4	6.5889	1.05907	0.72	<0.03	6.933
4.) ^{123}Te	1.2	2.2831	0.41794	12.1	<0.03	9.424
5.) ^{124}Te	5.0	13.181	2.15549	0.98	<0.03	6.571
6.) ^{125}Te	2.2	5.5059	0.92125	2.48	<0.02	9.120
7.) no sample						
8.) ^{126}Te	4.0	10.257	3.91742	3.17	<0.02	6.290

a samples of 10 mm diameter except ^{126}Te (15 mm diameter)

b for samples 3-8 sum of all Te isotopes (oxygen not included)

c % of weight

d Impurity of other elements except oxygen

sample. The sample masses of the main isotopes, ^{122,123,124}Te, are lower in weight by factors of 3 to 14 compared to the samples used by Macklin and Winters[7]. Hence, sample-related uncertainties, i.e. for multiple scattering and self-shielding corrections, are significantly reduced. The heavier isotopes, ^{125}Te and ^{126}Te, were included in the measurement to correct the data of the other samples for isotopic impurities.

The exact characterization of the sample is a severe problem for accurate cross section measurements[11]. This was particularly difficult in the case of tellurium, due to the oxygen affinity of this element . Another problem is a possible contamination with hydrogen in the form of water or a hydrite[12] . Therefore, the material was carefully analysed to detect contaminations of these two elements. The sample material was stored in a glove box under argon atmosphere, the samples were welded into thin polyethylene foils during the experiment, and their weight was controlled before and after the measurement to check for oxygen absorption. These precautions were necessary since dummy samples from

natural tellurium powder showed an increase in weight of 0.3 % per week when stored in air.

The sample material was checked via gas analysis of solids using the method of vacuum hot extraction. For this purpose, 10 mg powder was molten under vacuum in a graphite container together with a bath material (2g ultrapure Sn) at a temperature of 2300 °C. The tellurium metal forms an alloy with the bath material. Hydrogen, either in the form of a hydrite or absorbed as water, is released into the gaseous phase. The same happens to oxygen impurities, which react with the graphite to form CO . The hydrogen is detected in the gaseous phase by measuring the heat conductivity and the CO by infrared absorption. The apparatus is calibrated by gases with well defined composition. The method was optimized and checked using natural tellurium oxyde. Two (and in case of ^{123}Te three) independent measurements have been performed for each sample material to prove the reproducibility of the method and the homogeneity of the powder. The results are compiled in Table II. Unfortunately the "metallic" ^{123}Te powder supplied by ORNL was strongly oxydized, while the other isotopes which we had on loan from the USSR were in much better shape. In any case, data analysis simply adopting the specified metallicity of the supplyer would have led to desasterous errors in the cross section. Hydrogen was not detected in the sample material. It should be stressed that such problems with unexpected sample impurities may well be one of the reasons for the discrepancies in neutron capture cross section measurements that can be found in literature.

The isotopic composition was redetermined at KfK with two thermion mass separators, one with a 90 deg magnetic sector field, and the other with an electric quadrupol analyser. The results are compiled in Table III together with the data provided by the suppliers. In general good agreement is found , the only significant differences being observed for the isotopes 122 and 123 in the ^{122}Te sample (see Sec. V).

The diameter of the samples is 10 mm. In case of ^{126}Te, the sample mass of 4 g made it necessary to increase the diameter to 15 mm. As can be seen from Table II, the thickness of some samples is comparatively large and the transmission is only 0.92 (see Table IV). Since accurate data for the total cross section of the tellurium isotopes were not available from literature, the spectra measured with the neutron monitor at 260 cm flight path did not allow to check the normalization of the neutron flux as in our first measurement (Ref. 10).

TABLE III. Isotopic enrichment of the tellurium samples [%].

Sample	Isotope 120	122	123	124	125	126	128	130	
^{122}Te	<0.01	91.2	1.23	1.91	0.80	1.57	1.91	1.38	USSR
	<0.01	91.86	0.61	1.77	0.78	1.58	1.98	1.42	KfK
^{123}Te	<0.02	0.54	89.39	1.59	1.24	2.72	2.53	1.99	ORNL
	<0.01	0.48	89.58	1.52	1.24	2.68	2.51	1.99	KfK
^{124}Te	<0.002	0.07	0.07	92.4	4.06	1.59	1.06	0.75	USSR
	<0.01	<0.2	<0.1	92.61	4.03	1.55	1.07	0.74	KfK
^{125}Te	<0.006	<0.006	<0.006	0.88	93.9	3.61	1.06	0.55	USSR
	<0.01	<0.05	<0.03	0.90	93.88	3.55	1.07	0.60	KfK
^{126}Te	<0.026	<0.026	0.08	0.09	0.16	98.4	0.93	0.34	USSR
	<0.01	<0.02	<0.01	0.07	0.17	98.58	0.85	0.34	KfK

Matrix for the isotopic correction [%][a].

Corrected Spectrum	Measured Spectrum ^{122}Te	^{123}Te	^{124}Te	^{125}Te	^{126}Te	Corrected Sample Thickness [10^{-3} At/barn]
^{122}Te	100	-1.966	-0.9450	-0.8805	-0.7932	6.0523
^{123}Te	-0.1817	100	-0.2799	-0.5137	-0.4223	2.0451
^{124}Te	-	-	100	-10.2678	-1.1833	12.2016
^{125}Te	-	-	-0.4050	100	-1.0078	5.1664
^{126}Te	-	-	-0.1297	-0.7451	100	10.1601

[a] using the approximation $\sigma(^{128}Te) = 0.5 \times \sigma(^{126}Te)$ and $\sigma(^{130}Te) = 0.2 \times \sigma(^{126}Te)$

TABLE IV. Transmission of the samples [a].

Sample	Neutron energy [keV]				
	10	20	40	100	200
Au	0.933	0.942	0.949	0.958	0.965
^{122}Te	0.960	0.960	0.960	0.959	0.958
^{123}Te	0.969	0.972	0.974	0.975	0.976
^{124}Te	0.924	0.925	0.924	0.922	0.921
^{125}Te	0.961	0.963	0.965	0.966	0.966
^{126}Te	0.941	0.942	0.942	0.942	0.941

[a] Monte Carlo calculation with SESH code

All samples were welded into 10 μm thick polyethylene foils. This was nesessary to prevent losses during the experiment, when the samples are cycled into the measuring position in short intervals, and to avoid absorption of oxygen in the tellurium samples. The unwanted hydrogen introduced in this way results in a transmission of the foil of 0.9984, and to a slightly moderated neutron flux at the position of the sample. However, this effect cancels out to a large extent in the present experiment since samples and reference sample are affected in the same way due to their similar cross section shapes.

C. MEASUREMENTS

A computer controlled sample changer moved the samples cyclically into the measuring position. The data acquisition time per sample was about 10 min, completing one cycle in about 1.5 h. From each event, a 64 bit word was recorded on magnetic tape containing the sum energy and TOF information together with 42 bits indicating those detector modules that have contributed. As mentioned above, three runs have been performed using neutron spectra with different maximum energy. The essential parameters are compiled in Table V. In run I, the threshold in the sum energy spectrum was lowered to 1.9 MeV, while in the

TABLE V. Parameters of the individual measurements.

Run	Flight path [mm]	Time calibration [ns/channel]	Number of cycles	Maximum neutron energy [keV]	Measuring time [h]	Average beam current [μA]	Sum energy threshold [MeV]
I	786.3	0.7372	200	100	345	1.5	1.9
II	786.1	0.7330	258	200	351	2.0	2.4
III	786.1	0.7334	255	70	440	1.7	2.4

other runs it was fixed at 2.4 MeV. This threshold determines the recorded event rate, which was ~1 kHz for the lower and 500 Hz for the higher threshold. In total, ~200 high density tapes of data containing roughly 30 Gbyte of information were recorded during this experiment. The spectra of the two neutron monitor detectors were stored on disk.

III. DATA EVALUATION

The data evaluation has been described in detail in Ref. 10. All events stored on magnetic tape were sorted into two-dimensional sum energy versus TOF spectra according to event multiplicities (evaluation 1). In evaluation 2, this procedure was repeated by rejecting those events, where only neighboring detector modules contributed to the sum energy signal, in order to reduce background from the natural radioactivity of the BaF_2 crystals and from capture of scattered neutrons in the scintillator material. These spectra were normalized to equal neutron flux using the count rate from the lithium glass monitor, which was located close to the neutron target; these normalization factors are in general well below 1% (see Sec. V). In the next step, the spectra measured without sample were subtracted to remove the sample-independent background. The remaining time-independent background was determined at very long flight times (~3.9 μs), where no time-correlated events are expected. Two-dimensional spectra of run I and II containing all events with multiplicity >2 are shown in Fig. 2.

At this point, the spectra contain only events that are correlated with the sample. Now the correction for isotopic impurities can be performed. Since data were taken from five tellurium isotopes simultaneously, a set of five linear equations can be solved exactly. The coefficients are compiled in the lower part of Table III. The isotopes ^{128}Te and ^{130}Te, not covered by the present experiment, were treated as ^{126}Te, since this isotope has about the same binding energy. The cross section ratio was assumed to be energy-independent and to scale as 1 : 0.5 : 0.2 for ^{126}Te : ^{128}Te : ^{130}Te according to Ref. 13. The impurities of these isotopes are in the percent range and their cross sections are small. Therefore, this assumption does not affect the results. The coefficients in the correction matrix are all of the order of 1 % except the correction for ^{125}Te in the spectrum measured with the ^{124}Te sample (~10 %). But even in this case, the countrate in the TOF spectrum was affected by 4 % at maximum: Because the binding energy of ^{125}Te is large, most of the capture events fall in a sum energy range (>7.5 MeV) that is not used for the determination of the ^{124}Te cross section at all.

In the corrected spectrum, calculated e.g. for ^{122}Te from the five measured spectra and using the matrix elements given in Table III, not only the isotopic impurities of ^{123}Te to ^{126}Te are eliminated, but also the effect of the main isotope is reduced. This is because the spectra measured with the other samples contain ^{122}Te as an impurity. In the final analysis, this was considered by a corrected sample thickness, that is given in the last column of Table III.

After the correction for isotopic impurities, the background due to capture of sample scattered neutrons was removed from the spectra by means of the data measured with the carbon sample. The scattered neutrons are captured mainly in the barium isotopes of the scintillator material. This is shown in Fig. 3, where the sum energy of the events recorded with the graphite sample is plotted. The binding energy of the even tellurium isotopes being below 7 MeV, capture events in ^{135,137}Ba are well separated by their sum energy from the true capture events in the sample. The energy range from 8 to 10 MeV (dashed box in Fig. 3) is used to normalize the carbon spectrum for subtraction of the sample scattered neutron background. This normalization is calculated in dependence of the TOF, which is very important for the accuracy of the experimental method. After subtraction, the spectra contain true capture events only (lower part of Fig. 2), and can be used to determine the cross section.

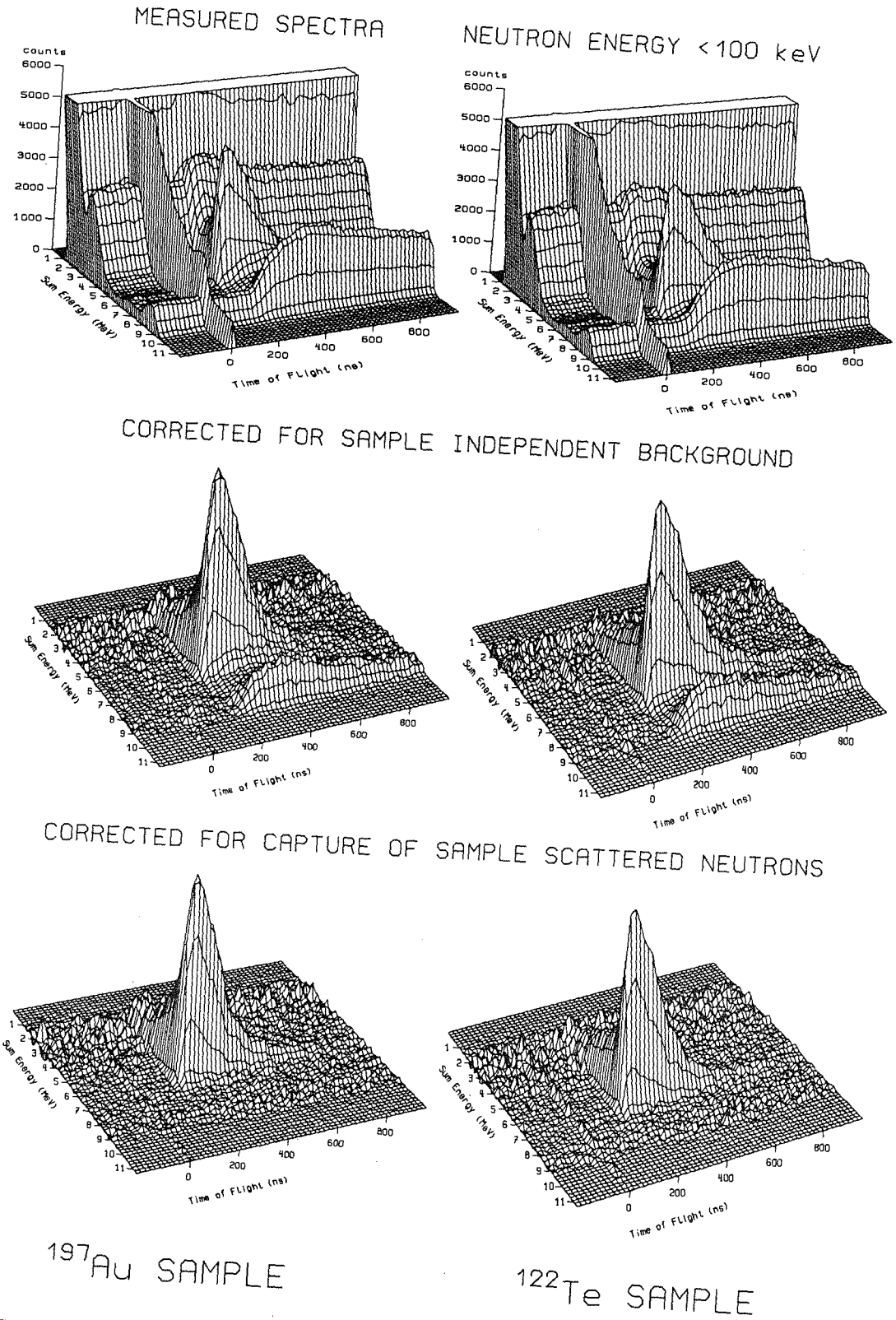

Fig. 2a The different steps of background subtraction in the two-dimensional sum energy × TOF spectra. The data are shown for the s-only tellurium isotopes and the gold

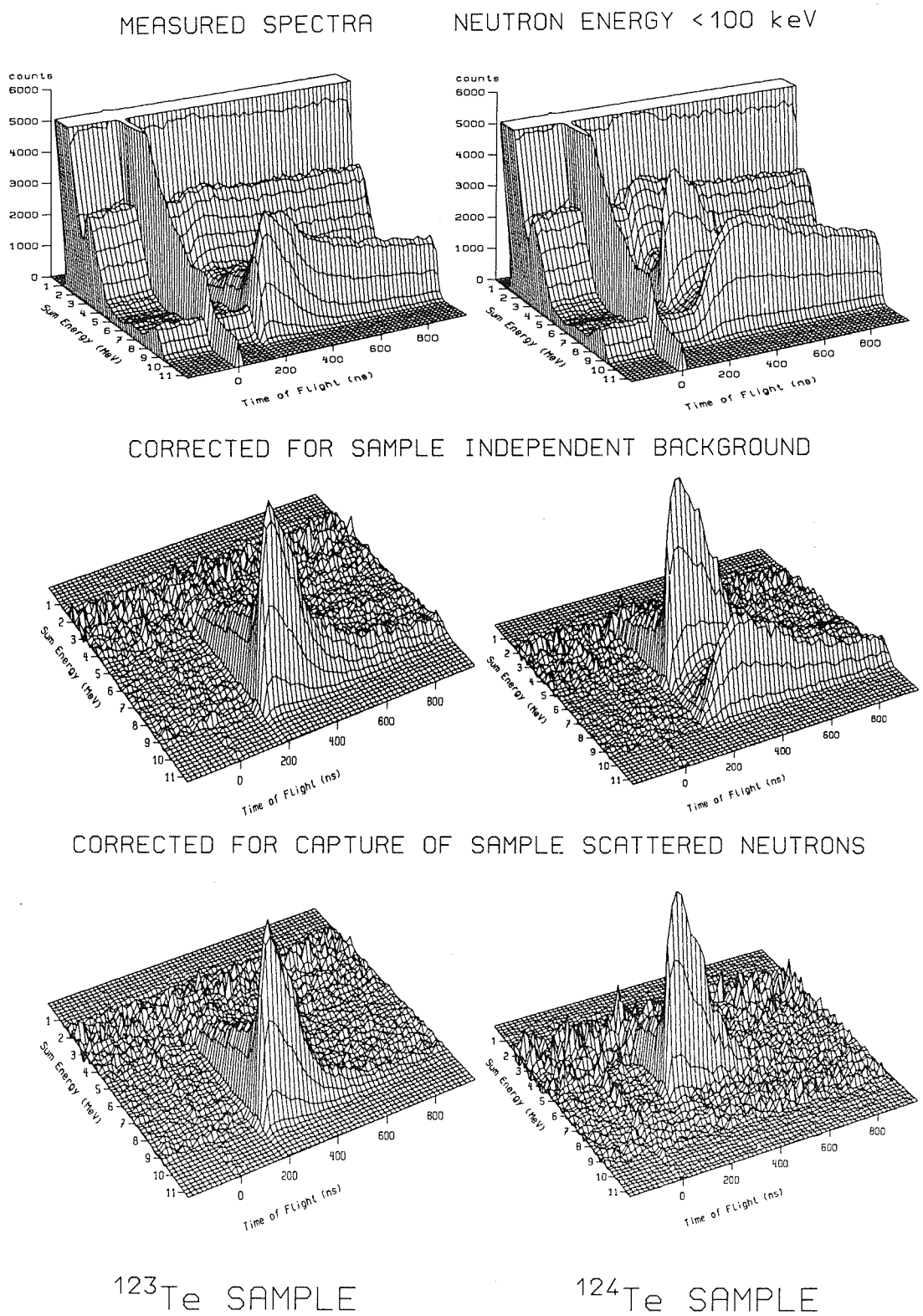

standard measured in run I with 100 keV maximum neutron energy. (Multiplicity >2. The original resolution of 128×2048 channels was compressed in the plots into 64×64 channels.)

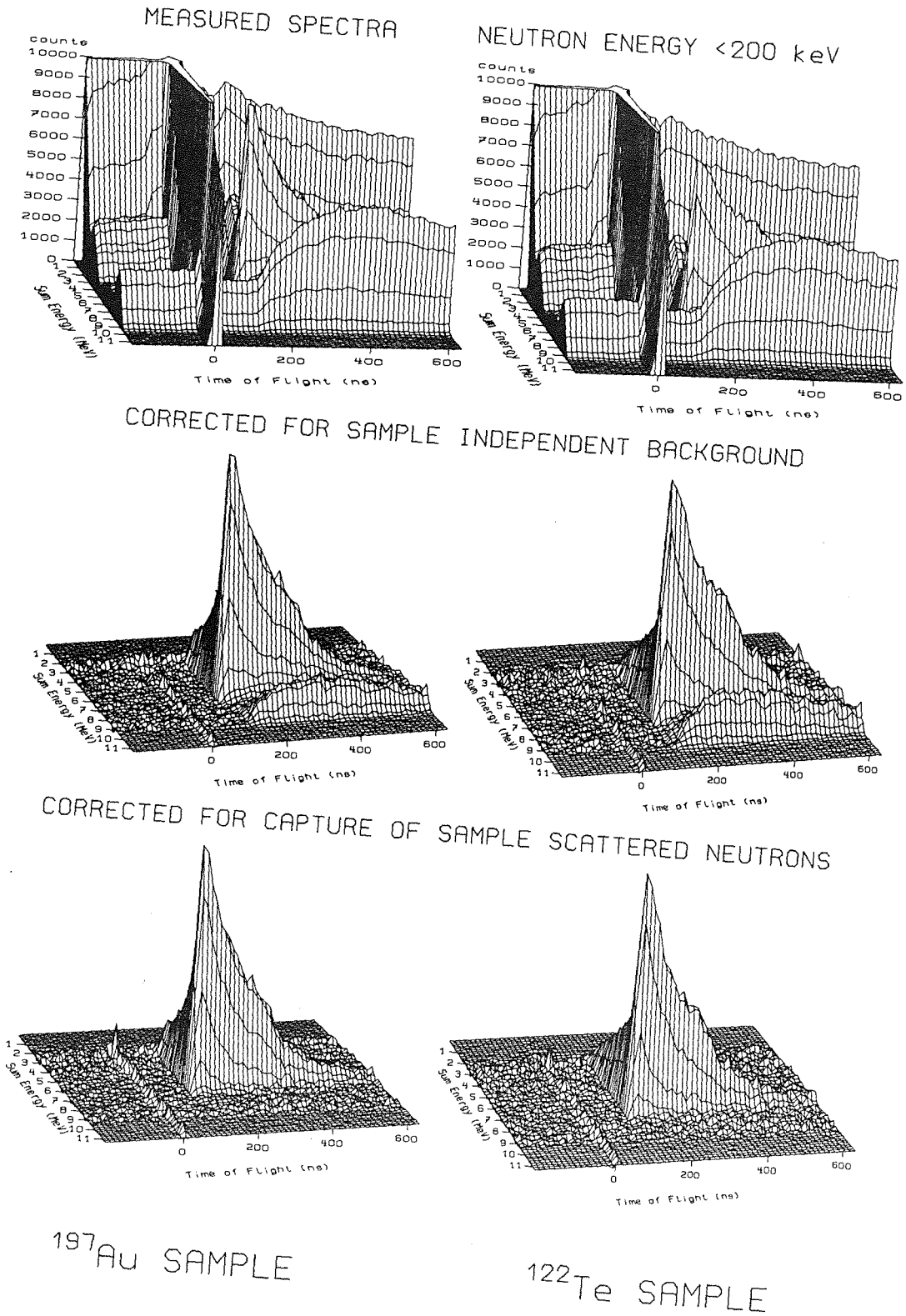

Fig. 2b The same as Fig. 2a but for run II with maximum neutron energy of 200 keV.

MEASURED SPECTRA

NEUTRON ENERGY <200 keV

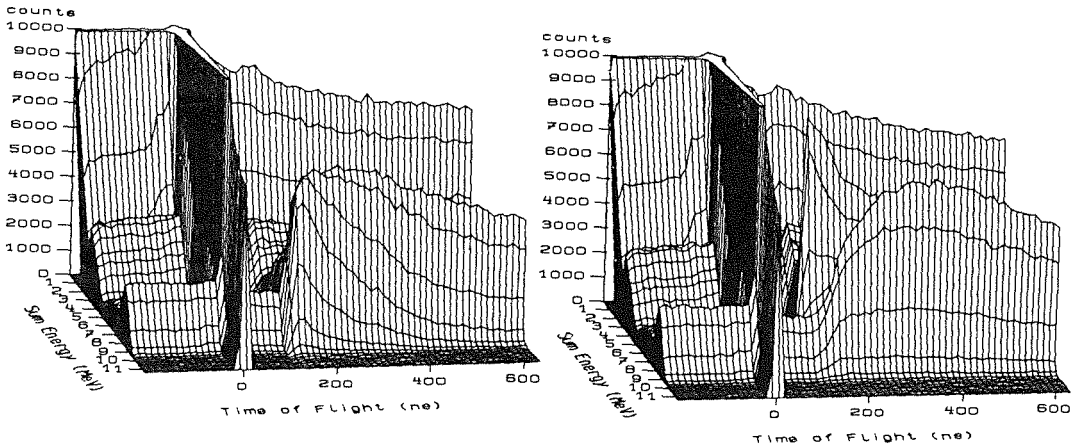

CORRECTED FOR SAMPLE INDEPENDENT BACKGROUND

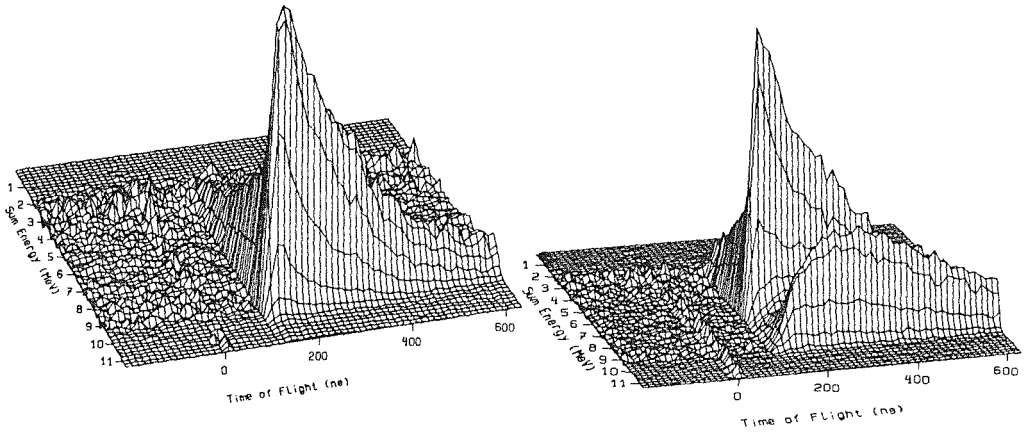

CORRECTED FOR CAPTURE OF SAMPLE SCATTERED NEUTRONS

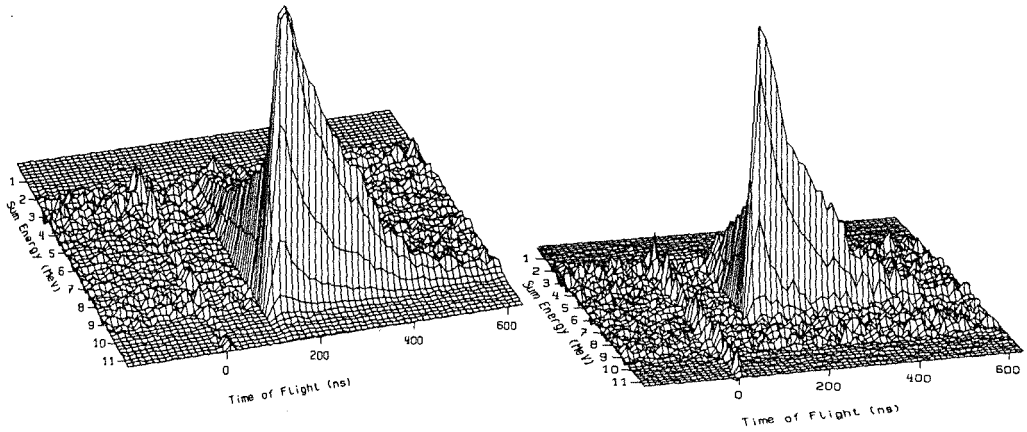

^{123}Te SAMPLE

^{124}Te SAMPLE

MEASURED SPECTRA

NEUTRON ENERGY <100 keV NEUTRON ENERGY <200 keV

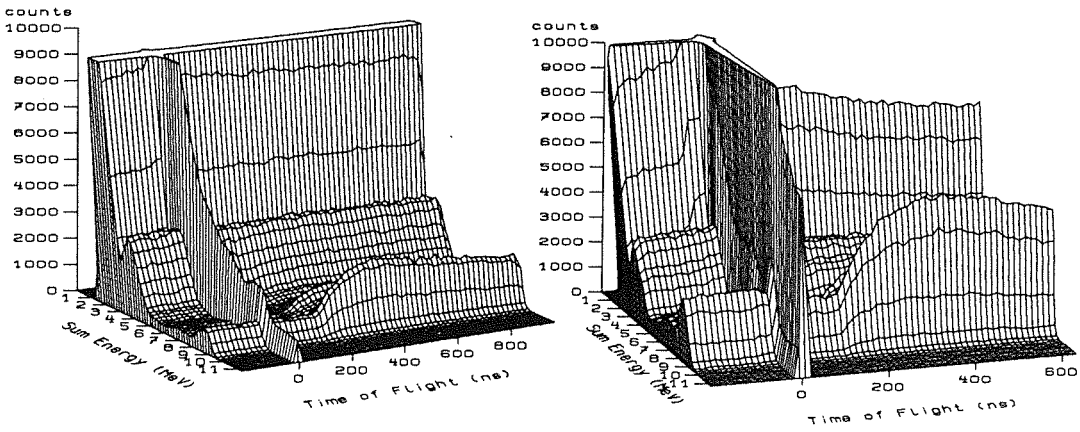

CORRECTED FOR SAMPLE INDEPENDENT BACKGROUND

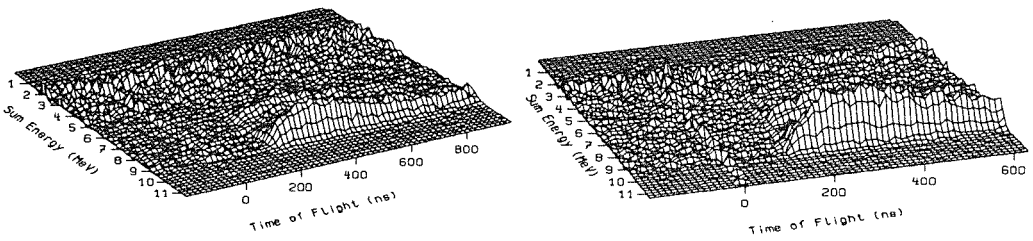

^{12}C SAMPLE ^{12}C SAMPLE

Fig. 2c The respective spectra measured with the carbon sample to simulate the background due to capture of sample scattered neutrons in the BaF_2 scintillator of the detector.

For the odd tellurium isotopes, this procedure is not applicable since their binding energy is ~9 MeV. In this case, the correction for sample scattered neutrons has to be normalized at the peak due to capture in ^{134}Ba and ^{136}Ba (see Fig. 3), which was integrated for several TOF intervals . This method, however, leads to systematic uncertainties at very low neutron energies because of the reduced signal-to-background ratio. For the odd isotopes the cross section was , therefore, evaluated only above 15 keV neutron energy.

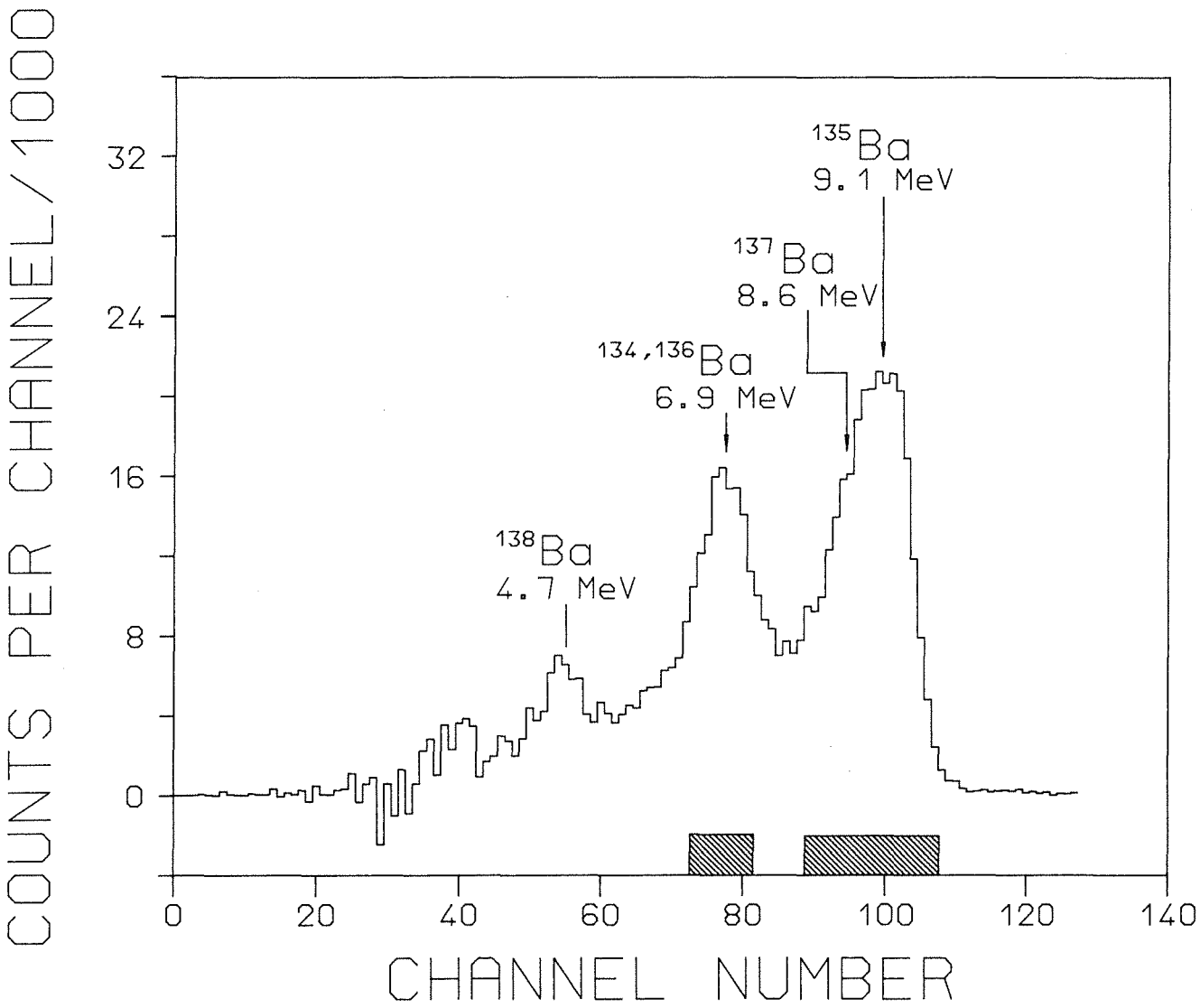

Fig. 3 Sum energy spectrum measured with the graphite sample, showing capture events in the different barium isotopes of the scintillator. The hatched boxes indicate the range that was used to normalize the corresponding background for the odd (left) and even (right) tellurium isotopes, respectively.

In Fig. 4, the TOF spectra of the ^{122}Te sample are plotted after projection of the two-dimensional data in the sum energy range around the binding energy (see below). The background due to capture of sample scattered neutrons is shown separately. The data are given for the three experimental runs with 200, 100 and 70 keV maximum neutron energy . Note, that the signal to background ratio at 30 keV increases from 4.0 to 5.7 and 7.4, respectively. At low neutron energies, the signal to background ratio is rapidly decreasing.

In view of the comparably small cross sections of the isotopes investigated here, it is, therefore, not possible to extend the evaluation below 10 keV with sufficient statistical accuracy.

In Table VI, the signal to background ratio is compiled for the s-only tellurium isotopes as well as for the gold standard in more detail. In spite of the fact that the ratio of total and capture cross sections, σ_t/σ_γ is quite different for the individual tellurium isotopes, there are no significant differences in the signal to background ratio. This can be understood if the respective binding energies are taken into account. In case of ^{122}Te, the binding energy coincides exactly with the binding energy of the even barium isotopes (6.9 MeV). Thus the capture peak is found at the position of the ^{134}Ba, ^{136}Ba peak in the carbon spectrum (see Fig. 3). For ^{124}Te, the binding energy is significantly lower (6.6 MeV). Hence, the larger σ_t/σ_γ ratio is compensated by the fact that part of the capture events in the even barium isotopes could be discriminated by selecting an appropriate upper threshold in the sum energy. In contrast, the high binding energy of ^{123}Te does not allow for a significant suppression of the background and consequently a comparatively low signal to background ratio is obtained in spite of the favorable total to capture ratio. In addition, the high oxygen content of this sample contributes nearly 30 % of the background.

The data in Table VI demonstrate that the optimum signal to background ratio at 30 keV neutron energy is obtained in the run with lowest maximum neutron energy. It is interesting to note, however, that the signal to background ratio at 10 keV is about equal in the runs with 100 and 70 keV maximum energy. The higher background due to the larger integral neutron flux at 100 keV is compensated by the fact that also the effect is larger due to the higher neutron flux compared to the run with 70 keV maximum energy.

After subtraction of the background the TOF spectra shown in Fig. 4 were used to determine the shape of the cross section. For normalization, the two-dimensional spectra were projected on the sum energy axis in the region of optimum signal to background ratio as indicated by dashed boxes in Fig. 4 . The result is shown in Fig. 5 where the events with multiplicity >2 are plotted for all isotopes.

In Fig. 6, the sum energy spectra of the s-only isotopes and of the gold standard are shown in dependence of the detector multiplicity. A multiplicity ≧5 is observed for ~40 % of the events in the even and for ≧60 % in the odd tellurium isotopes. Gamma-ray background

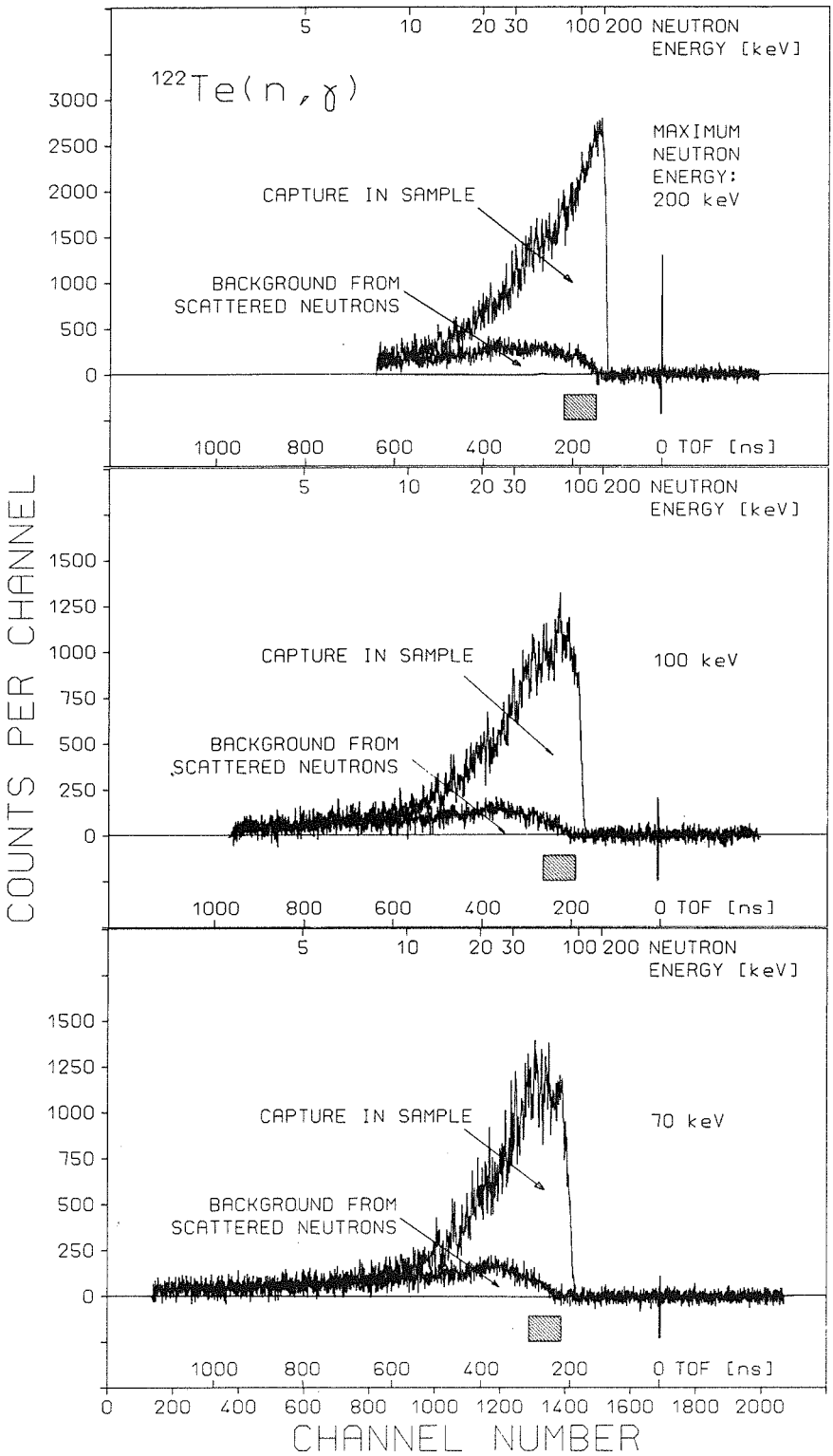

Fig. 4 TOF spectra measured with the ^{122}Te sample in runs with different maximum neutron energy. The background due to capture of sample scattered neutrons is shown separately. The signal to background ratio at 30 keV increases from 4.0 to 5.7 and 7.4 by lowering the maximum neutron energy (see Table VI). The region used for the absolute normalization of the cross section is shown by hatched boxes.

TABLE VI. Signal to background ratio in dependence of neutron energy for runs with different maximum neutron energy

Sample	σ_t/σ_γ at 30 keV	Maximum neutron energy [keV]	Signal to background ratio Neutron Energy [keV] 30	20	10
^{122}Te	21	70	7.4	3.7	1.6
^{123}Te	14		6.6	2.9	1.5
^{124}Te	40		5.5	2.9	1.6
Au	24		13.4	4.7	2.2
^{122}Te		100	5.7	3.5	1.6
^{123}Te			5.1	2.7	1.7
^{124}Te			4.0	2.7	1.6
Au			9.3	4.5	2.4
^{122}Te		200	4.0	2.6	1.4
^{123}Te			3.7	2.3	1.4
^{124}Te			3.0	1.9	1.3
Au			6.4	3.3	1.9

affects mainly the spectra with multiplicity 1 and 2 below ~3 MeV (channel number 40) giving rise to large statistical fluctuations. The figure demonstrates the potentials of the detector as a multiplicity filter that separates capture events with high multipliciy from gamma-ray background with low multiplicity.

The cross section ratio of isotope X relative to the gold standard is then:

$$\frac{\sigma_l(X)}{\sigma_l(Au)} = \frac{Z_l(X)}{Z_l(Au)} \times \frac{\Sigma Z(Au)}{\Sigma Z(X)} \times \frac{\Sigma E(X)}{\Sigma E(Au)} \times \frac{m(Au)}{m(X)} \times F_1 \times F_2 . \qquad (1)$$

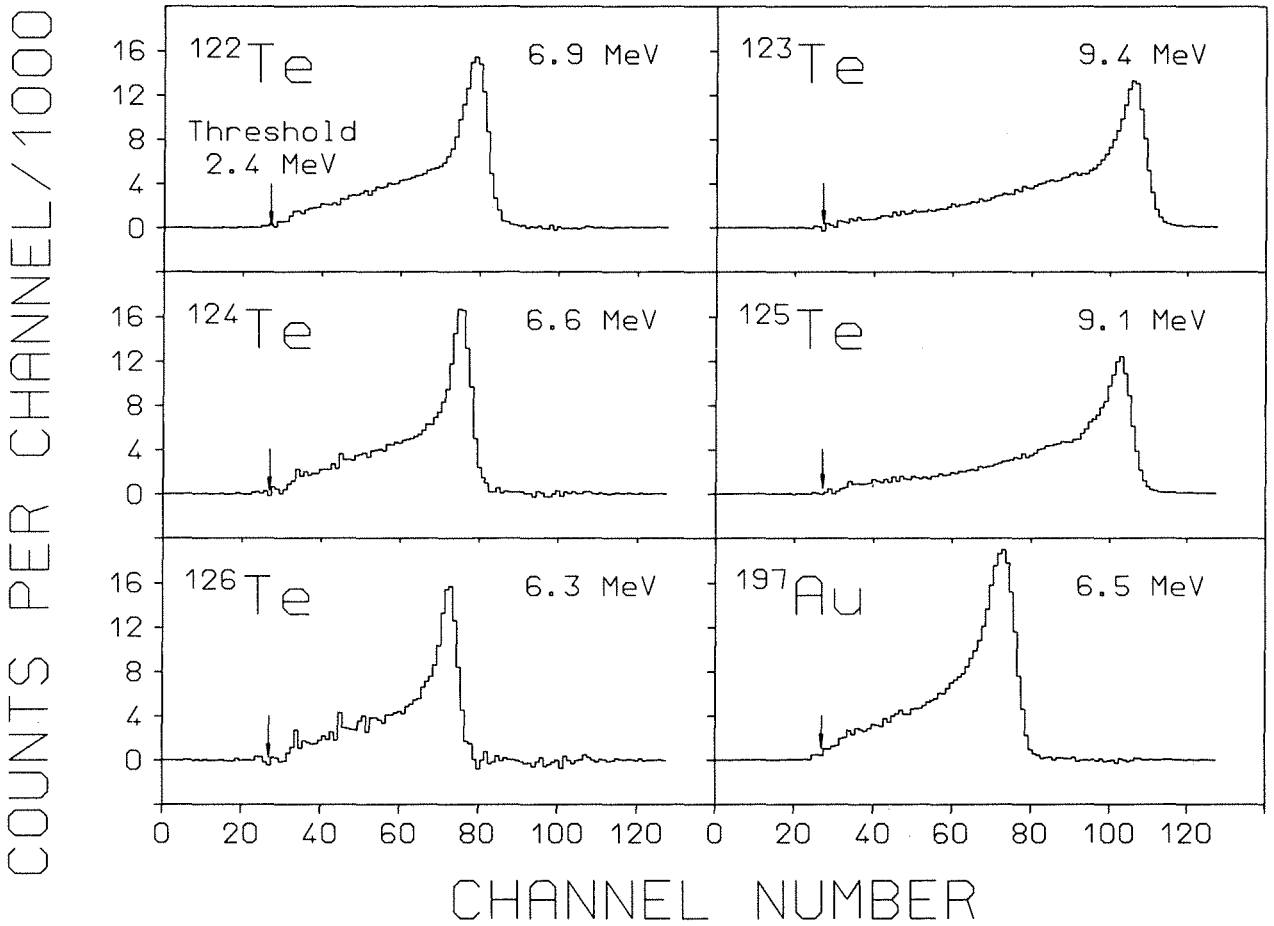

Fig. 5 Sum energy spectra of all isotopes measured in run II containing all events with multiplicity >2. These spectra were obtained by projection of the two-dimensional spectra in the TOF region below the maximum neutron energy as indicated for the ^{122}Te sample in Fig. 4.

In this relation, Z_i is the countrate in channel i of the TOF spectrum, ΣZ is the integral TOF count rate in the interval used for normalization (see Fig. 4), ΣE is the total count rate in the sum energy spectrum for all multiplicities summed over the normalization interval (see Fig. 6), and m is the sample thickness in atom/barn. The correction factor F_1 is the ratio of the capture events below the threshold for sample and reference sample (Table VII), and F_2 the respective ratio of the multiple scattering corrections.

The fraction of unobserved capture events, f and the correction factor F_1 were calculated as described in detail in Ref. 10. For this purpose, two informations are necessary: the individual neutron capture cascades and their relative contribution to the total capture

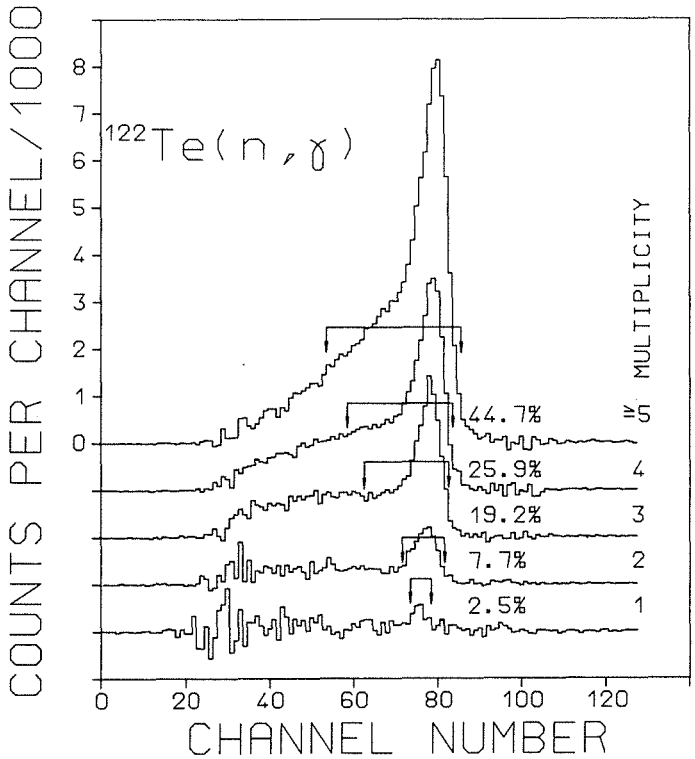

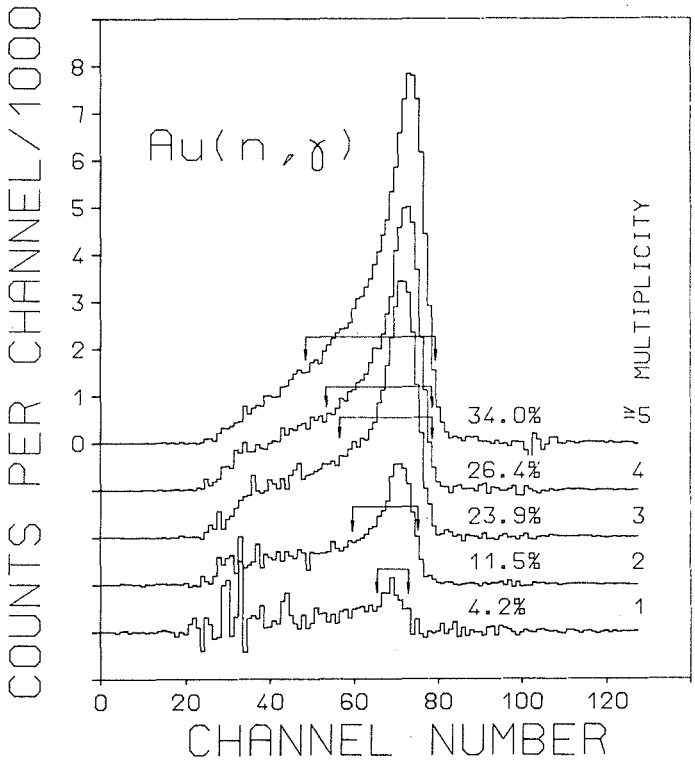

Fig. 6 Sum energy spectra from the s-only tellurium isotopes and the gold sample in dependence of detector multiplicity (the same data as shown in Fig. 5). The regions used to determine the cross section shape are indicated by arrows.

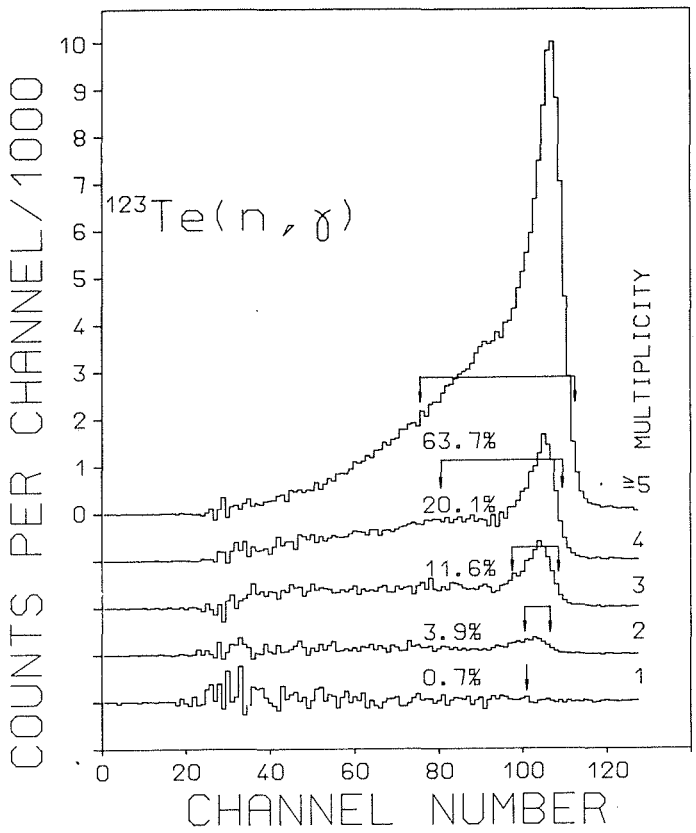
^{123}Te(n,γ)
COUNTS PER CHANNEL/1000
CHANNEL NUMBER
MULTIPLICITY
≥ 5
4
3
2
1
63.7%
20.1%
11.6%
3.9%
0.7%

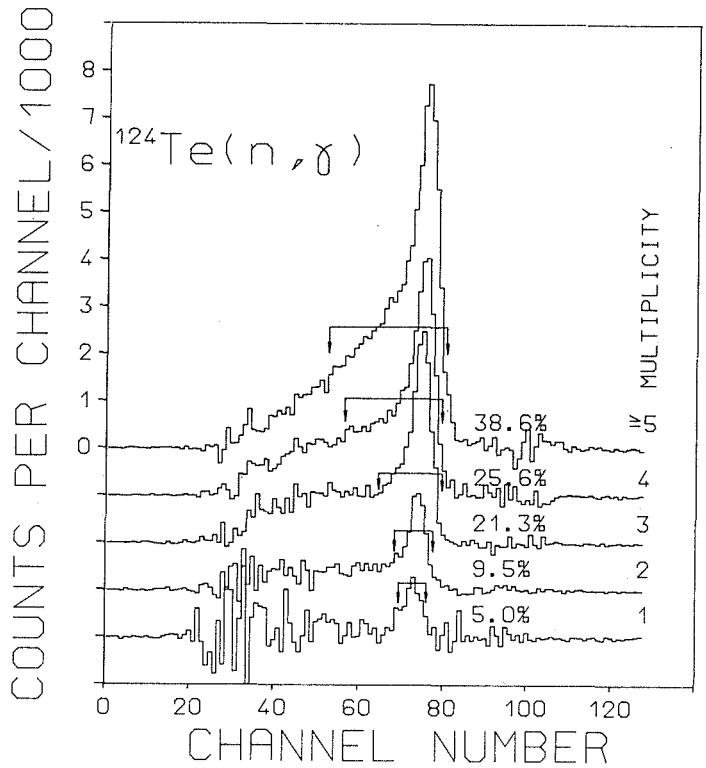
^{124}Te(n,γ)
COUNTS PER CHANNEL/1000
CHANNEL NUMBER
MULTIPLICITY
≥ 5
4
3
2
1
38.6%
25.6%
21.3%
9.5%
5.0%

cross section as well as the detector efficiency for monoenergetic gamma-rays in the energy range up to 10 MeV.

The capture cascades and capture gamma-ray spectra of the involved isotopes have been calculated according to the statistical and optical model[14]. In Table VIII, the cross section is given as a function of the cascade multiplicity together with the gamma-ray energies of the 20 most probable cascades. The respective data for gold have been given already in Ref. 10. The first 20 cascades yield 25 to 35 % of the cross section, but up to 1000 are necessary to cover 95 %. The average multiplicity of the cascades ranges from 3.2 to 3.8. The capture gamma-ray spectra are given in Fig. 7.

The efficiency of a BaF_2 shell for monoenergetic gamma-rays was calculated in Ref. 15 with different assumptions for multiple Compton events, resulting in an optimistic and a pessimistic estimate for the peak efficiency SW(MAX) and SW(MIN). The data given in Ref. 10 were used to calculate the fraction f of unobserved capture events (see Table VII). In the actual measurements, we used a threshold in the sum energy of 1.9 MeV in run I and of 2.4 MeV in runs II and III. Accordingly, the efficiency of the detector was 97-98 % for the odd and 93-95 % for the even isotopes. It has to be noted that for the present experimental method it is not necessary to know the absolute efficiency of the detector, which depends on the efficiency for monoenergetic gamma-rays. As can be seen from Table VII, differences of the order of 1 % are observed for the different assumptions SW(MAX) and SW(MIN). Since sample and standard are measured with the same detector, the final correction factors F_1 are quite insensitive to the assumed detector efficiency. For the even isotopes, which are close in binding energy to the gold standard , the correction is very small and only for the odd isotopes differences in efficiency of several % are found.

In Fig. 8, the calculated sum energy spectra are shown separately for the two different assumptions of the detector efficiency. Comparison with the experimental results given in Fig. 5 demonstrate that they are indeed between these two extremes.

The correction for multiple scattering and self-shielding in the sample was calculated by the SESH code[16]. Recently, the code was changed by the author to consider the more accurate formula for the level density as described already in Ref. 10 . The parameter of nuclear temperature was replaced by the pairing energy Δ which was taken from Ref. 17. Now, the level spacing of p- and d-waves is calculated by the program . The main problem is to find sets of parametes that reproduce not only the capture cross section but, in

TABLE VII. Calculated fraction of unobserved capture events, f (%), and the corresponding correction factors, F_1 , for the cross section ratios.

Sample	Threshold in sum energy [MeV]					Assumption for gamma-ray efficiency
	1.5	1.9	2.0	2.4	2.5	
Solid angle 94 %, gamma-ray threshold 50 keV						
f(Au)	3.66		5.25		7.78	SW(MAX)
f(^{122}Te)	3.07		5.22		6.88	
f(^{123}Te)	1.27		1.89		3.30	
f(^{124}Te)	3.15		5.10		6.93	
f(^{125}Te)	1.00		1.48		2.27	
f(^{126}Te)	3.16		6.72		8.85	
f(Au)	4.08		6.19		8.99	SW(MIN)
f(^{122}Te)	3.63		5.89		8.95	
f(^{123}Te)	1.48		2.50		3.81	
f(^{124}Te)	3.70		5.87		8.40	
f(^{125}Te)	1.14		1.82		2.63	
f(^{126}Te)	4.02		7.45		9.93	
F_1(^{122}Te/Au)	0.995	0.997	0.998	0.996	0.995	$^1/_2$SW(MAX)+
F_1(^{123}Te/Au)	0.975	0.967	0.964	0.953	0.950	$^1/_2$SW(MIN)
F_1(^{124}Te/Au)	0.996	0.997	0.998	0.993	0.992	
F_1(^{125}Te/Au)	0.971	0.962	0.959	0.943	0.939	
F_1(^{126}Te/Au)	0.997	1.010	1.015	1.012	1.011	

TABLE VIII. Calculated capture gamma-ray cascades including multiplicities, partial cross sections, σ_p, and gamma-ray energies of the 20 most significant cascades.

^{122}Te

σ(30 keV)=0.300 b	total capture cross section
σ(mul 1)=0.0054 b	
σ(mul 2)=0.0414 b	
σ(mul 3)=0.0996 b	
σ(mul 4)=0.0975 b	average multiplicity <m>=3.6
σ(mul 5)=0.0458 b	
σ(mul 6)=0.0103 b	
σ(mul 7)=0.0000 b	

calculated number of cascades: 1000 (covering 94.6 % of the cross section)

σ_p [mbarn]	σ_p/σ_{tot} [%]	gamma1	gamma2	gamma3 [MeV]	gamma4	gamma5
6.12	2.04	5.276	1.686			
5.63	1.88	5.276	1.527	0.159		
5.40	1.80	6.963				
4.84	1.61	6.804	0.159			
4.60	1.53	4.690	2.114	0.159		
4.44	1.48	4.690	2.273			
4.02	1.34	4.104	2.700	0.159		
3.65	1.22	4.104	2.859			
3.55	1.18	3.518	3.286	0.159		
3.42	1.14	6.363	0.600			
3.26	1.09	6.523	0.440			
3.11	1.04	3.518	3.445			
2.99	1.00	2.931	3.872	0.159		
2.62	0.87	6.458	0.505			
2.57	0.86	2.931	4.031			
2.25	0.75	2.345	4.459	0.159		
2.22	0.74	2.931	2.345	1.527	0.159	
2.16	0.72	4.690	1.833	0.440		
2.16	0.72	2.931	2.345	1.686		
2.14	0.71	4.104	2.419	0.440		
	Σ 23.7%					

TABLE VIII. (continued)

^{123}Te

σ(30 keV)=0.900 b	total capture cross section
σ(mul 1)=0.0203 b	
σ(mul 2)=0.0945 b	
σ(mul 3)=0.2460 b	
σ(mul 4)=0.2943 b	average multiplicity <m>=3.8
σ(mul 5)=0.1859 b	
σ(mul 6)=0.0590 b	
σ(mul 7)=0.0000 b	

calculated number of cascades: 1000 (covering 94.8 % of the cross section)

σ_p [mbarn]	σ_p/σ_{tot} [%]	gamma1	gamma2	gamma3 [MeV]	gamma4	gamma5
20.3	2.25	9.454				
20.2	2.24	8.851	0.603			
14.8	1.65	6.525	2.326	0.603		
14.1	1.57	5.800	3.051	0.603		
13.9	1.54	5.075	3.776	0.603		
13.7	1.52	4.350	4.501	0.603		
12.9	1.44	3.625	5.226	0.603		
11.0	1.22	2.900	5.951	0.603		
9.97	1.11	6.525	2.929			
9.71	1.08	2.900	3.625	2.326	0.603	
9.64	1.07	3.625	2.900	2.326	0.603	
8.82	0.98	8.128	0.723	0.603		
8.78	0.98	7.717	1.737			
8.49	0.94	8.298	0.553	0.603		
8.33	0.93	5.800	3.654			
7.74	0.86	2.175	6.676	0.603		
7.67	0.85	4.350	2.175	2.326	0.603	
7.66	0.85	5.075	4.379			
7.49	0.83	2.175	4.350	2.326	0.603	
7.41	0.82	4.350	5.104			
	Σ=24.7%					

TABLE VIII. (continued)

^{124}Te

σ(30 keV)=0.170 b	total capture cross section
σ(mul 1)=0.0044 b	
σ(mul 2)=0.0257 b	
σ(mul 3)=0.0547 b	
σ(mul 4)=0.0536 b	average multiplicity <m>=3.5
σ(mul 5)=0.0240 b	
σ(mul 6)=0.0076 b	
σ(mul 7)=0.0000 b	

calculated number of cascades: 557 (covering 95 % of the cross section)

σ_p [mbarn]	σ_p/σ_{tot} [%]	gamma1	gamma2	gamma3 [MeV]	gamma4	gamma5
4.88	2.87	5.235	1.332	0.035		
4.37	2.57	6.602				
4.34	2.55	6.567	0.035			
4.25	2.50	4.654	1.913	0.035		
3.89	2.29	4.072	2.495	0.035		
3.71	2.18	5.235	1.367			
3.54	2.08	3.490	3.077	0.035		
3.21	1.89	4.654	1.948			
3.03	1.78	2.909	3.658	0.035		
2.92	1.72	4.072	2.530			
2.66	1.56	3.490	3.112			
2.30	1.35	2.327	4.240	0.035		
2.28	1.34	2.909	3.693			
2.23	1.31	2.909	2.327	1.332	0.035	
2.06	1.21	3.490	1.745	1.332	0.035	
2.01	1.18	5.873	0.694	0.035		
1.98	1.16	2.327	2.908	1.332	0.035	
1.97	1.16	6.158	0.444			
1.73	1.02	2.327	4.275			
1.55	0.91	2.909	2.327	1.367		
	Σ=34.6%					

TABLE VIII. (continued)

^{125}Te

σ(30 keV)=0.570 b total capture cross section
σ(mul 1)=0.0128 b
σ(mul 2)=0.0585 b
σ(mul 3)=0.1443 b
σ(mul 4)=0.1854 b average multiplicity <m>=3.8
σ(mul 5)=0.1256 b
σ(mul 6)=0.0434 b
σ(mul 7)=0.0000 b

calculated number of cascades: 1000 (covering 94.1 % of the cross section)

σ_p [mbarn]	σ_p/σ_{tot} [%]	gamma1	gamma2	gamma3 [MeV]	gamma4	gamma5
12.8	2.25	5.047	3.435	0.666		
12.8	2.24	9.148				
12.6	2.21	5.678	2.804	0.666		
12.1	2.13	4.417	4.066	0.666		
10.7	1.88	3.786	4.696	0.666		
9.75	1.71	8.482	0.666			
8.66	1.52	3.155	5.327	0.666		
8.27	1.45	3.155	2.523	2.804	0.666	
8.09	1.42	5.047	4.101			
7.92	1.39	5.678	3.470			
7.81	1.37	4.417	4.732			
7.58	1.33	2.524	3.155	2.804	0.666	
7.07	1.24	3.786	1.893	2.804	0.666	
7.01	1.23	3.786	5.363			
6.27	1.10	2.524	5.958	0.666		
5.93	1.04	3.155	5.993			
5.53	0.97	2.524	2.524	3.435	0.666	
5.36	0.94	1.893	3.785	2.804	0.666	
5.02	0.88	3.155	2.523	3.470		
4.90	0.86	3.155	1.893	3.435	0.666	
	Σ=29.2 %					

TABLE VIII. (continued)

^{126}Te

σ(30 keV)=0.085 b	total capture cross section	
σ(mul 1)=0.0025 b		
σ(mul 2)=0.0203 b		
σ(mul 3)=0.0336 b		
σ(mul 4)=0.0206 b	average multiplicity	<m>=3.2
σ(mul 5)=0.0064 b		
σ(mul 6)=0.0016 b		
σ(mul 7)=0.0000 b		

calculated number of cascades: 611 (covering 95.0 % of the cross section)

σ_p [mbarn]	σ_p/σ_{tot} [%]	gamma1	gamma2	gamma3 [MeV]	gamma4	gamma5
3.05	3.59	4.968	1.352			
2.46	2.89	6.320				
2.43	2.86	4.416	1.904			
2.30	2.71	6.259	0.061			
2.07	2.43	3.864	2.456			
1.78	2.09	3.312	3.008			
1.70	2.00	4.968	1.291	0.061		
1.45	1.71	2.760	3.560			
1.40	1.65	4.416	1.843	0.061		
1.31	1.54	5.556	0.764			
1.22	1.44	3.864	2.395	0.061		
1.16	1.36	2.760	2.208	1.352		
1.09	1.28	3.312	1.656	1.352		
1.09	1.28	3.312	2.947	0.061		
1.07	1.26	2.208	4.112			
1.00	1.18	2.208	2.760	1.352		
0.92	1.08	2.760	3.499	0.061		
0.87	1.02	5.817	0.503			
0.84	0.99	5.847	0.473			
0.84	0.98	3.864	1.104	1.352		
	Σ=35.3 %					

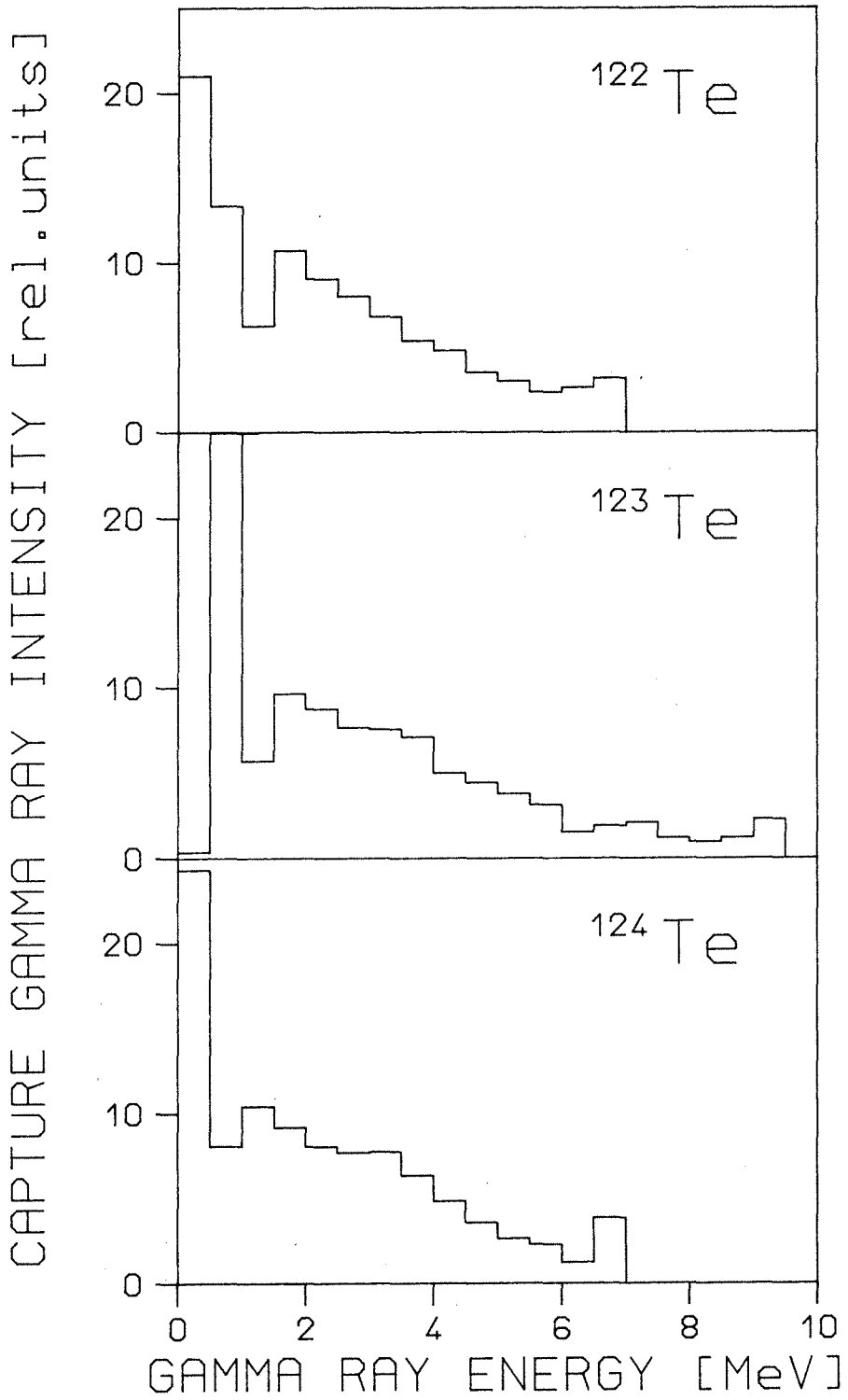

Fig. 7 Calculated capture gamma-ray spectra for the s-only tellurium isotopes.

addition, the total cross section of each isotope as well. It proved, that experimental results on the total cross section were not available in the energy range considered. Data were published only above 200 keV in the work of Musaelyan and Skorkin[18] . Therefore, the calculations were made in three different ways in order to find the most reliable results and to study the sensitivity on the input parameters.

In the first calculation, we started from the parameters given by Mughabghab[19]. These data were changed such that the total cross section of the JEF evaluation[20] was reproduced within an uncertainty of ~3 % and the capture cross sections of Macklin and Winters[7] within ~10 %. The respective input parameters as well as the results for the total cross sections are compiled in Table IX.

In the second step, a detailed resonance analysis was performed using the possibilities of the Bologna group, i.e. analysis of the cumulative number of neutron width distributions, of the cumulative number of resonances, of the reduced neutron widths, the reduced neutron width sampling analysis, the truncated Porter Thomas distribution and the missing level estimator method. These studies led to a recommended set of parameters (Table X) which gave significantly larger total cross sections (see Table IX). This input was only slightly modified in order to reproduce the capture cross sections.

Finally, the total cross sections were measured for the s-only isotopes in the energy range from 10 to 80 keV in a separate experiment[21] together with the shape of the capture cross section which was determined down to 1 keV. In this experiment, good agreement was found with the JEF data for ^{122}Te and ^{124}Te , while for ^{123}Te the cross section was significantly larger. Therefore, a third calculation was performed for this isotope increasing the S_o strength function. The parameters are compiled in Table IX. The stars in the last line indicate those sets that were used for the final correction.

In case of ^{123}Te, oxygen was included in the calculation. The contamination of 12.1 % in weight (see Table II) leads to a contribution of 1.06 oxygen atoms per tellurium atom which causes a significant increase of the total cross section. The individual results for the multiple scattering correction MS(X) are compiled in Table XI . Most severe differences were found at low energies. Above 10 keV neutron energy, the range which was covered by the present experiment, the differences are minor but still not negligible if uncertainties of the order of 1 % are aimed at for the cross section ratio. Especially, if one would rely in the case of ^{123}Te on the evaluated JEF data and/or would neglect the oxygen content of the

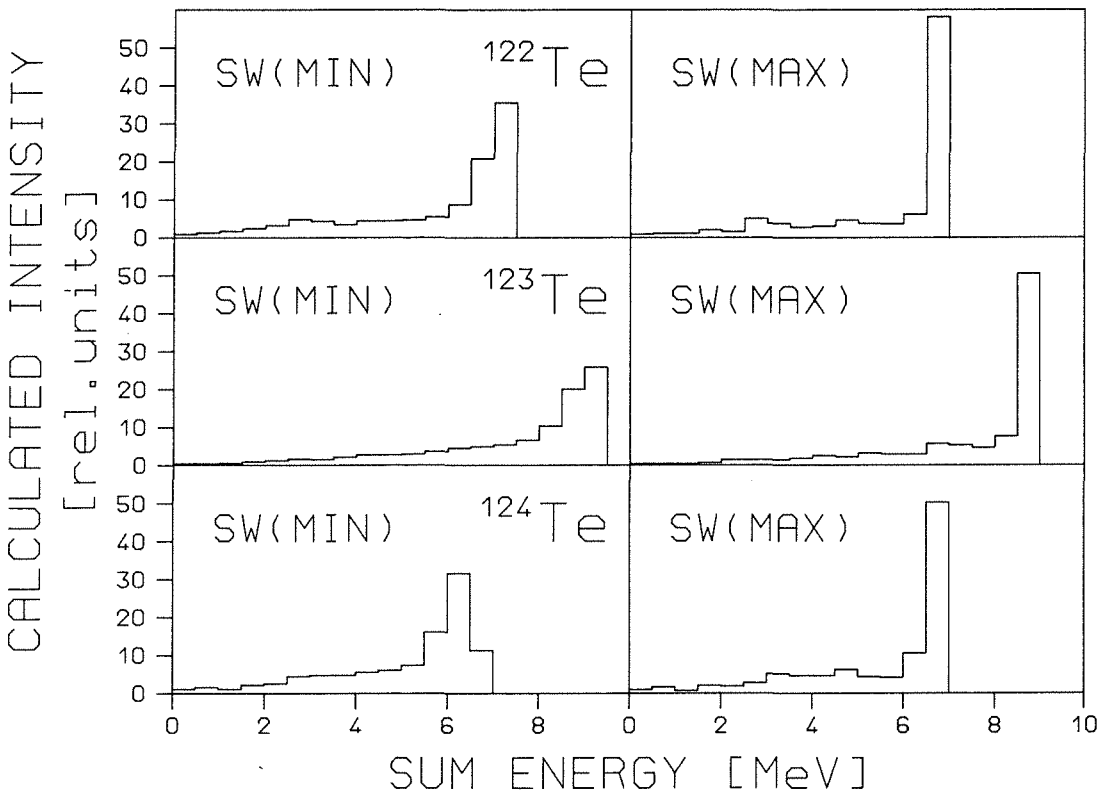

Fig. 8 Calculated sum energy spectra of the 4π BaF_2 detector as obtained under different assumptions on the detector efficiency. These spectra were used to derive the correction F_1 for unobserved capture events.

sample, significant systematic uncertainties would result for the data. The correction factors MS(X) adopted in the final evaluation as well as the correction factors F_2 are compiled in Table XII.

The comparatively small sample masses used in the present experiment lead still to sizable corrections up to ~5 % . In the work of Macklin and Winters[7], which was carried out with samples that were up to 12 times heavier , no data are given for this correction. In view of the problems outlined above it seems that the quoted uncertainty of 1.3 % is rather optimistic at least at energies below 10 keV where the corrections exceed 20 %.

The determination of the neutron energy could be checked by means of the ^{126}Te resonances at low neutron energies, as shown by the TOF spectrum in Fig. 9. On average, the energy of the channel with maximum intensity agreed with the resonance energies given by Macklin and Winters[7] to better than 100 eV.

TABLE IX. Input parameters for the calculation of neutron multiple scattering and self-shielding corrections with SESH[16]. Two parameter sets are given for each Te isotope and three for ^{123}Te.

Parameter		Isotope											
		^{122}Te			^{123}Te		^{124}Te		^{125}Te		^{126}Te		^{16}O
Nucleon number		122			123		124		125		126		16
Abundance		1			1		1		1		1		1
Binding energy[MeV]		6.933			9.424		6.571		9.120		6.290		4.144
Pairing E. [MeV]		1.14			2.57		1.14		2.23		1.14		0.0
Eff.temp.[K]		293			293		293		293		293		293
Nucl.spin		0			1/2		0		1/2		0		0
Av.rad.width	s	0.100	0.120	0.350	0.200	0.150	0.025	0.070	0.157	0.155	0.002	0.050	0.0
[eV]	p	0.100	0.120	0.150	0.200	0.200	0.050	0.100	0.048	0.155	0.055	0.050	0.0
Av. levelsp.	s	132	200	25	27	27	130	310	38	56	210	330	0
[eV]													
Strength fct.	S_0	0.38	0.70	0.4	0.7	1.3	0.4	0.69	0.48	0.7	0.5	0.7	0
[10^{-4}]	S_1	3.0	3.0	2.8	2.8	2.8	2.6	2.6	2.4	2.4	2.2	2.2	0
Nucl. radius	s	5.7	5.7	5.7	5.7	5.7	5.7	5.7	5.7	5.7	5.6	5.7	5.5
[fm]													
Calculated total cross section													
Neutron Energy [keV]													
3		7.40	9.80	7.52	9.78	14.28	7.49	9.67	8.06	9.72	8.04	9.69	3.80
6		6.72	8.41	6.79	8.37	11.53	6.75	8.27	7.13	8.29	7.05	8.24	3.80
10		6.43	7.71	6.45	7.66	10.08	6.40	7.57	6.67	7.56	6.56	7.50	3.79
20		6.24	7.12	6.23	7.05	8.71	6.15	6.95	6.30	6.91	6.15	6.83	3.77
40		6.26	6.85	6.20	6.75	7.84	6.10	6.64	6.15	6.55	5.96	6.46	3.74
100		6.49	6.79	6.37	6.65	7.21	6.23	6.51	6.17	6.38	5.93	6.23	3.64
200		6.67	6.80	6.51	6.63	6.81	6.35	6.47	6.22	6.31	5.96	6.15	3.49
in agreement with		JEF	Reffo	JEF	Reffo	Xia	JEF	Reffo	JEF	Reffo	JEF	Reffo	
finally adopted:		*				*	*			*	*		

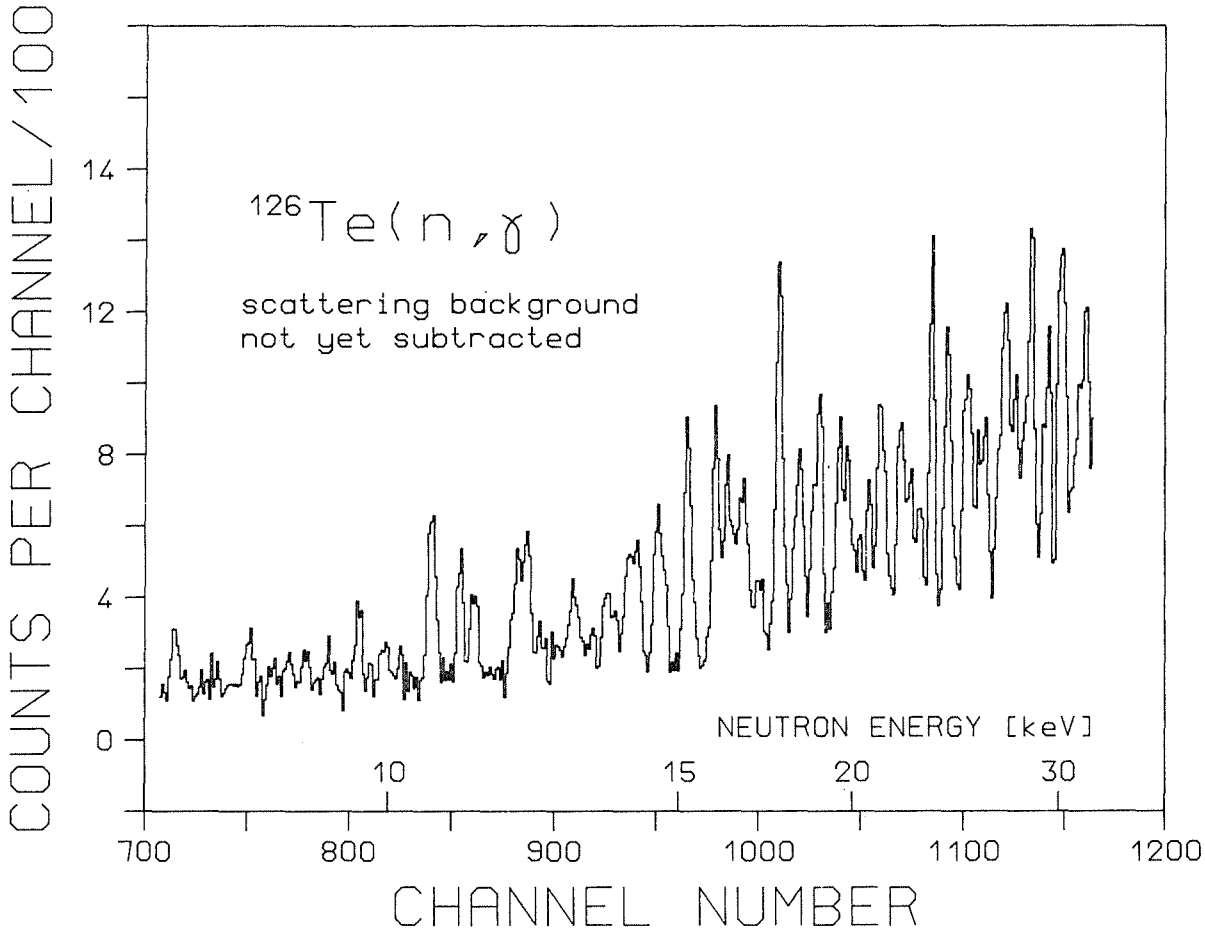

Fig. 9 TOF spectrum measured with the ^{126}Te sample at low neutron energies. This spectrum was used to check the neutron energy callibration.

TABLE X. Recommended statistical parameters for the tellurium isotopes.

	N	D [eV]	Γ_n^o [eV]	S_o [$\times 10^{-4}$]	Γ_γ [eV]	ν
^{122}Te	50±5	200±50	0.017±0.03	$0.9\,^{0.6}_{1.3}$	152±36	6
^{123}Te	71±5	$29\,^{2.7}_{3.1}$	0.0035±0.0005	1.0±0.3	111±8	20
^{124}Te	95±5	260±50	0.02	0.66±0.03	152±36	
^{125}Te	132±9	56.2±7	0.0036±0.0001	0.6±0.1	155±11	20
^{126}Te	51±3	350±20	0.01	0.28±0.02		

TABLE XI. Correction factors for neutron multiple scattering and self-shielding, MS, calculated under different assumptions for the total cross section of the tellurium isotopes (see Table IX). In case of ^{123}Te the values calculated for the observed oxygen content are given, too.

	Neutron Energy [keV]						
Sample	3	6	10	20	40	100	200
Au	0.926	0.987	1.012	1.035	1.038	1.031	1.022
Total Cross Section accordind to JEF (Ref. 20)							
^{122}Te	0.871	0.940	0.966	0.988	0.996	1.002	1.006
^{123}Te	0.972	0.988	0.998	1.002	1.004	1.003	1.001
^{123}Te + O	0.979	0.996	1.006	1.009	1.010	1.008	1.006
^{124}Te	0.860	0.921	0.945	0.957	0.969	0.985	0.992
^{125}Te	0.922	0.966	0.984	0.998	1.003	1.007	1.006
^{126}Te	0.934	0.955	0.965	0.973	0.977	0.987	0.997
Total Cross Section according to evaluation of Reffo (see Table X)							
^{122}Te	0.815	0.911	0.951	0.978	0.991	0.999	1.005
^{123}Te	0.963	0.986	0.999	1.003	1.004	1.004	1.004
^{123}Te + O	0.970	0.994	1.005	1.009	1.010	1.009	1.007
^{124}Te	0.752	0.845	0.890	0.936	0.962	0.979	0.995
^{125}Te	0.888	0.953	0.979	0.999	1.006	1.008	1.009
^{126}Te	0.762	0.867	0.912	0.945	0.964	0.984	1.009
Total Cross Section according to measurement of Xia et al. (Ref. 21)							
^{123}Te	0.952	0.985	1.002	1.006	1.006	1.006	1.004
^{123}Te + O	0.958	0.991	1.005	1.009	1.011	1.009	1.008

TABLE XII. Correction factors for neutron multiple scattering and self-shielding, MS, and the related correction factors, F_2 = MS(Au)/MS(X) for the cross section ratio.

Energy range [keV]	MS					
	Au	^{122}Te	^{123}Te	^{124}Te	^{125}Te	^{126}Te
5 - 10	0.997	0.952	0.997	0.933	0.965	0.960
10 - 15	1.020	0.975	1.007	0.950	0.986	0.968
15 - 20	1.031	0.985	1.009	0.956	0.995	0.972
20 - 30	1.037	0.991	1.010	0.961	1.002	0.975
30 - 40	1.038	0.995	1.011	0.967	1.005	0.976
40 - 60	1.036	0.998	1.010	0.974	1.007	0.979
60 - 80	1.034	1.000	1.010	0.979	1.008	0.983
80 - 100	1.031	1.002	1.010	0.983	1.008	0.985
100 - 120	1.029	1.002	1.009	0.986	1.008	0.988
120 - 150	1.026	1.003	1.009	0.988	1.009	0.991
150 - 200	1.023	1.003	1.008	0.990	1.009	0.995

	F_2				
	Correction for Cross Section Ratio				
	^{122}Te/Au	^{123}Te/Au	^{124}Te/Au	^{125}Te/Au	^{126}Te/Au
5 - 10	1.047	1.000	1.069	1.033	1.039
10 - 15	1.046	1.013	1.074	1.034	1.054
15 - 20	1.047	1.022	1.078	1.036	1.061
20 - 30	1.046	1.027	1.079	1.035	1.064
30 - 40	1.043	1.027	1.073	1.033	1.064
40 - 60	1.038	1.026	1.064	1.029	1.058
60 - 80	1.034	1.024	1.056	1.026	1.052
80 - 100	1.029	1.021	1.049	1.023	1.047
100 - 120	1.027	1.020	1.044	1.021	1.041
120 - 150	1.023	1.017	1.038	1.017	1.035
150 - 200	1.020	1.015	1.033	1.014	1.028
Accuracy [%]	0.4	0.4	0.4	0.4	0.8

IV. RESULTS FOR THE NEUTRON CAPTURE CROSS SECTIONS.

The neutron capture cross section ratios of the tellurium isotopes relative to ^{197}Au are listed together with the respective statistical uncertainties in Tables XIII to XVII. The data are given for the three runs and the two evaluations discussed in Sec. III. The last column of the tables contains the weighted average, the weight being determined by the square of the statistical uncertainties. Since the cross section ratios depend weakly on energy, the averages for the energy interval from 30 to 100 keV are also included which allows for a better comparison of the individual results. The statistical uncertainty quoted in this broad energy bin is a lower limit since it is only the uncertainty of the normalization factor:

$$N = (\Sigma Z(Au) \times \Sigma E(X))/(\Sigma Z(X) \times \Sigma E(Au)) \qquad (2)$$

from equation 1 that dominates over the uncertainty of the countrate Z_i. The differences in the uncertainties of this normalization factor documents that it is really worth while to reduce the background by the selection criterion chosen in evaluation 2. No systematic differences can be found in the data as obtained from different evaluations or different runs.

As in our first experiment[10] the results of evaluation 2 were adopted as the final cross section ratios. They are compiled together with statistical, systematic and total uncertainties in Table XVIII. The chosen energy binning allows an easy comparison with the data of Macklin and Winters[7]. The final uncertainty in the cross section ratio is of the order of 1 % and even the small cross section of ^{126}Te could be determined with ~2 % accuracy. This is a significant improvement compared to other experimental techniques. The Maxwellian averaged cross sections (see Sec. VI) were calculated from narrower energy intervals to avoid systematic uncertainties that are given in Table XIX .

The experimental ratios were converted into absolute cross sections by means of the gold cross section of Macklin[22] after normalization by a factor of 0.989 to the absolute value of Ratynski and Käppeler[23]. If these data, given in Table XX, are used in further work, their uncertainties can be calculated from the uncertainty of the cross section ratio by adding quadratically the 1.5 % uncertainty of the standard.

In Fig. 10 a comparison is made for the s-only isotopes to the data of Macklin and Winters[7]. On average, the agreement in the energy interval 20 to 100 keV is better than 2.5 %, well within the quoted uncertainties. The shape of the ^{125}Te cross section is slightly different.

TABLE XIII. The neutron capture cross section ratios $\sigma(^{122}Te)/\sigma(Au)$, and the respective statistical uncertainties in (%).

Energy range [keV]	Run I		Run II		Run III		Average	
Evaluation 1								
5 - 10	0.4039	9.0	-	-	0.4601	9.0	0.4321	6.3
10 - 15	0.5115	4.5	0.5091	4.7	0.4858	3.8	0.5000	2.5
15 - 20	0.5802	3.2	0.5804	3.2	0.6004	2.5	0.5892	1.7
20 - 30	0.5206	2.2	0.5311	1.8	0.5310	1.8	0.5284	1.1
30 - 40	0.5315	2.0	0.5419	1.5	0.5455	1.7	0.5407	1.0
40 - 60	0.5201	1.8	0.5282	1.2	0.5292	1.5	0.5267	0.8
60 - 80	0.5255	1.8	0.5245	1.2	0.5362	1.7	0.5277	0.9
80 - 100	0.5083	2.0	0.5302	1.2	-	-	0.5241	1.0
100 - 120	-	-	0.5127	1.2	-	-	0.5127	1.2
120 - 150	-	-	0.5218	1.1	-	-	0.5218	1.1
150 - 200	-	-	0.5475	1.1	-	-	0.5475	1.1
30 - 100	0.5214	1.6	0.5307	0.8	0.5366	1.4	0.5304	0.6
Evaluation 2								
5 - 10	0.3922	6.7	-	-	0.4580	6.9	0.4243	4.8
10 - 15	0.5115	3.4	0.4970	3.8	0.5054	3.0	0.5051	1.9
15 - 20	0.5969	2.4	0.6030	2.5	0.5994	2.0	0.5996	1.3
20 - 30	0.5285	1.6	0.5395	1.4	0.5386	1.3	0.5363	0.8
30 - 40	0.5322	1.5	0.5389	1.2	0.5533	1.2	0.5427	0.7
40 - 60	0.5211	1.3	0.5345	1.0	0.5352	1.1	0.5316	0.6
60 - 80	0.5281	1.3	0.5303	1.0	0.5408	1.3	0.5325	0.7
80 - 100	0.5114	1.5	0.5242	1.0	-	-	0.5202	0.8
100 - 120	-	-	0.5136	1.0	-	-	0.5136	1.0
120 - 150	-	-	0.5232	0.9	-	-	0.5232	0.9
150 - 200	-	-	0.5478	0.9	-	-	0.5478	0.9
30 - 100	0.5234	1.1	0.5315	0.6	0.5426	0.9	0.5329	0.5

TABLE XIV. The neutron capture cross section ratios $\sigma(^{123}Te)/\sigma(^{197}Au)$ and the respective statistical uncertainties in (%).

Energy range [keV]	Run I		Run II		Run III		Average	
Evaluation 1								
15 - 20	1.4045	3.6	1.5121	3.7	1.4693	2.9	1.4625	1.9
20 - 30	1.6014	2.2	1.5830	1.9	1.5515	1.8	1.5759	1.1
30 - 40	1.5870	2.0	1.5569	1.5	1.5374	1.7	1.5579	1.0
40 - 60	1.6143	1.8	1.6237	1.3	1.6146	1.6	1.6187	0.9
60 - 80	1.5895	1.8	1.5344	1.3	1.6080	1.8	1.5666	0.9
80 - 100	1.5615	1.9	1.5588	1.3	-	-	1.5597	1.1
100 - 120	-	-	1.4804	1.3	-	-	1.4804	1.3
120 - 150	-	-	1.4662	1.2	-	-	1.4662	1.2
150 - 200	-	-	1.3420	1.2	-	-	1.3420	1.2
30 - 100	1.5890	1.6	1.5692	0.9	1.5877	1.4	1.5772	0.7
Evaluation 2								
15 - 20	1.3822	2.9	1.4830	3.1	1.4288	2.3	1.4292	1.6
20 - 30	1.5994	1.7	1.5696	1.5	1.5402	1.4	1.5656	0.9
30 - 40	1.5754	1.5	1.5476	1.3	1.5541	1.2	1.5575	0.8
40 - 60	1.6288	1.2	1.6197	1.0	1.6261	1.1	1.6243	0.6
60 - 80	1.6048	1.2	1.5333	1.0	1.6092	1.3	1.5739	0.7
80 - 100	1.5837	1.4	1.5493	1.0	-	-	1.5608	0.8
100 - 120	-	-	1.4695	1.1	-	-	1.4695	1.1
120 - 150	-	-	1.4706	1.0	-	-	1.4706	1.0
150 - 200	-	-	1.3389	1.0	-	-	1.3389	1.0
30 - 100	1.6010	1.0	1.5638	0.6	1.5992	0.9	1.5799	0.4

TABLE XV. The neutron capture cross section ratios $\sigma(^{124}Te)/\sigma(^{197}Au)$ and the respective statistical uncertainties in (%).

Energy range [keV]	Run I		Run II		Run III		Average	
Evaluation 1								
5 - 10	0.2342	10.5	-	-	0.2508	10.2	0.2427	7.3
10 - 15	0.2346	6.3	0.2374	6.7	0.2445	4.9	0.2399	3.4
15 - 20	0.2910	4.1	0.3186	3.8	0.3334	3.0	0.3185	2.1
20 - 30	0.2717	3.0	0.2751	2.3	0.2786	2.3	0.2756	1.4
30 - 40	0.2716	2.7	0.2751	1.9	0.2699	2.2	0.2726	1.3
40 - 60	0.2736	2.5	0.2801	1.6	0.2785	2.0	0.2783	1.1
60 - 80	0.2521	2.5	0.2575	1.6	0.2630	2.3	0.2578	1.2
80 - 100	0.2726	2.7	0.2787	1.6	-	-	0.2771	1.3
100 - 120	-	-	0.2765	1.6	-	-	0.2765	1.6
120 - 150	-	-	0.2705	1.5	-	-	0.2705	1.5
150 - 200	-	-	0.2874	1.5	-	-	0.2874	1.5
30 - 100	0.2672	2.4	0.2728	1.2	0.2710	2.0	0.2715	0.9
Evaluation 2								
5 - 10	0.2161	8.8	-	-	0.2567	8.1	0.2381	6.0
10 - 15	0.2363	5.0	0.2479	5.2	0.2529	3.9	0.2469	2.7
15 - 20	0.3034	3.2	0.3185	3.1	0.3235	2.4	0.3167	1.6
20 - 30	0.2838	2.2	0.2866	1.8	0.2837	1.7	0.2847	1.1
30 - 40	0.2725	2.0	0.2736	1.5	0.2758	1.6	0.2742	1.0
40 - 60	0.2737	1.8	0.2802	1.3	0.2793	1.4	0.2785	0.8
60 - 80	0.2527	1.8	0.2599	1.3	0.2659	1.7	0.2599	0.9
80 - 100	0.2768	2.0	0.2750	1.3	-	-	0.2755	1.1
100 - 120	-	-	0.2763	1.3	-	-	0.2763	1.3
120 - 150	-	-	0.2730	1.2	-	-	0.2730	1.2
150 - 200	-	-	0.2893	1.2	-	-	0.2893	1.2
30 - 100	0.2686	1.6	0.2722	0.9	0.2744	1.3	0.2722	0.7

TABLE XVI. The neutron capture cross section ratios $\sigma(^{125}Te)/\sigma(^{197}Au)$ and the respective statistical uncertainties in (%).

Energy range [keV]	Run I		Run II		Run III		Average	
Evaluation 1								
15 - 20	0.9181	3.2	0.9509	3.3	0.9081	2.6	0.9226	1.7
20 - 30	1.0080	2.0	1.0196	1.7	0.9615	1.6	0.9938	1.0
30 - 40	0.9000	1.9	0.8988	1.5	0.8759	1.5	0.8908	0.9
40 - 60	0.8148	1.7	0.8122	1.3	0.8056	1.4	0.8106	0.8
60 - 80	0.6511	1.7	0.6503	1.3	0.6661	1.7	0.6548	0.9
80 - 100	0.6057	1.9	0.6228	1.3	-	-	0.6171	1.1
100 - 120	-	-	0.5465	1.4	-	-	0.5465	1.4
120 - 150	-	-	0.5081	1.3	-	-	0.5081	1.3
150 - 200	-	-	0.4771	1.3	-	-	0.4771	1.3
30 - 100	0.7446	1.5	0.7407	0.9	0.7914	1.3	0.7547	0.7
Evaluation 2								
15 - 20	0.8913	2.5	0.8985	2.7	0.8730	2.0	0.8850	1.4
20 - 30	0.9780	1.5	0.9940	1.4	0.9427	1.2	0.9686	0.8
30 - 40	0.8670	1.4	0.8699	1.2	0.8673	1.1	0.8681	0.7
40 - 60	0.8096	1.2	0.7970	1.0	0.7991	1.0	0.8011	0.6
60 - 80	0.6477	1.2	0.6377	1.0	0.6591	1.3	0.6467	0.7
80 - 100	0.6085	1.4	0.6072	1.1	-	-	0.6077	0.9
100 - 120	-	-	0.5312	1.1	-	-	0.5312	1.1
120 - 150	-	-	0.5009	1.0	-	-	0.5009	1.0
150 - 200	-	-	0.4695	1.0	-	-	0.4695	1.0
30 - 100	0.7372	1.0	0.7239	0.7	0.7864	0.9	0.7451	0.5

TABLE XVII. The neutron capture cross section ratios $\sigma(^{126}Te)/\sigma(^{197}Au)$ and the respective statistical uncertainties in (%).

Energy range [keV]	Run I		Run II		Run III		Average	
Evaluation 1								
5 - 10	0.1099	19.4	-	-	0.1265	18.6	0.1185	13.4
10 - 15	0.1379	9.5	0.1597	8.8	0.1428	8.0	0.1469	5.0
15 - 20	0.1875	6.3	0.2156	5.2	0.2152	5.3	0.2083	3.2
20 - 30	0.1420	5.5	0.1435	4.2	0.1441	4.8	0.1433	2.7
30 - 40	0.1293	5.3	0.1361	3.7	0.1325	4.7	0.1335	2.5
40 - 60	0.1392	5.0	0.1500	3.1	0.1408	4.5	0.1453	2.3
60 - 80	0.1232	5.0	0.1322	3.0	0.1276	4.8	0.1294	2.3
80 - 100	0.1297	5.2	0.1371	3.2	-	-	0.1351	2.7
100 - 120	-	-	0.1389	3.2	-	-	0.1389	3.2
120 - 150	-	-	0.1373	3.1	-	-	0.1373	3.1
150 - 200	-	-	0.1381	3.0	-	-	0.1381	3.0
30 - 100	0.1304	4.8	0.1388	2.7	0.1339	4.4	0.1361	2.1
Evaluation 2								
5 - 10	0.1057	17.1	-	-	0.1351	15.7	0.1217	11.6
10 - 15	0.1431	7.6	0.1569	7.5	0.1630	6.1	0.1557	4.0
15 - 20	0.2080	4.6	0.2171	4.2	0.2239	3.8	0.2174	2.4
20 - 30	0.1467	4.0	0.1446	3.3	0.1507	3.3	0.1474	2.0
30 - 40	0.1320	3.7	0.1321	2.9	0.1420	3.1	0.1356	1.8
40 - 60	0.1416	3.4	0.1471	2.4	0.1473	2.9	0.1459	1.6
60 - 80	0.1270	3.4	0.1324	2.4	0.1362	3.2	0.1321	1.7
80 - 100	0.1363	3.6	0.1361	2.4	-	-	0.1362	2.0
100 - 120	-	-	0.1385	2.4	-	-	0.1385	2.4
120 - 150	-	-	0.1395	2.3	-	-	0.1395	2.3
150 - 200	-	-	0.1426	2.2	-	-	0.1426	2.2
30 - 100	0.1343	3.2	0.1374	1.9	0.1423	2.8	0.1380	1.4

TABLE XVIII. The final neutron capture cross section ratios of ^{122}Te, ^{123}Te, ^{124}Te, ^{125}Te, and ^{126}Te relative to ^{197}Au together with the statistical and systematic uncertainties in (%).

Energy [keV]	$\sigma(^{122}Te)/\sigma(^{197}Au)$	uncertainty stat	sys	tot	$\sigma(^{123}Te)/\sigma(^{197}Au)$	uncertainty stat	sys	tot	$\sigma(^{124}Te)/\sigma(^{197}Au)$	uncertainty stat	sys	tot
5 - 10	0.4243	4.8	0.8	4.9	-	-	-	-	0.2381	6.0	0.8	6.1
10 - 15	0.5051	1.9	0.8	2.1	-	-	-	-	0.2469	2.7	0.8	2.8
15 - 20	0.5996	1.3	0.8	1.5	1.4292	1.6	0.8	1.8	0.3167	1.6	0.8	1.8
20 - 30	0.5363	0.8	0.8	1.1	1.5656	0.9	0.8	1.2	0.2847	1.1	0.8	1.4
30 - 40	0.5427	0.7	0.8	1.1	1.5575	0.8	0.8	1.1	0.2742	1.0	0.8	1.3
40 - 60	0.5316	0.6	0.8	1.0	1.6243	0.6	0.8	1.0	0.2785	0.8	0.8	1.1
60 - 80	0.5325	0.7	0.8	1.1	1.5739	0.7	0.8	1.1	0.2599	0.9	0.8	1.2
80 - 100	0.5202	0.8	0.8	1.1	1.5608	0.8	0.8	1.1	0.2755	1.1	0.8	1.4
100 - 120	0.5136	1.0	0.8	1.3	1.4695	1.1	0.8	1.4	0.2763	1.3	0.8	1.5
120 - 150	0.5232	0.9	0.8	1.2	1.4706	1.0	0.8	1.3	0.2730	1.2	0.8	1.4
150 - 200	0.5478	0.9	0.8	1.2	1.3389	1.0	0.8	1.3	0.2893	1.2	0.8	1.4

Energy [keV]	$\sigma(^{125}Te)/\sigma(^{197}Au)$	uncertainty stat	sys	tot	$\sigma(^{126}Te)/\sigma(^{197}Au)$	uncertainty stat	sys	tot
5 - 10	-	-	-	-	0.1217	11.6	1.0	11.6
10 - 15	-	-	-	-	0.1557	4.0	1.0	4.1
15 - 20	0.8850	1.4	0.8	1.6	0.2174	2.4	1.0	2.6
20 - 30	0.9686	0.8	0.8	1.1	0.1474	2.0	1.0	2.2
30 - 40	0.8681	0.7	0.8	1.1	0.1356	1.8	1.0	2.1
40 - 60	0.8011	0.6	0.8	1.0	0.1459	1.6	1.0	1.9
60 - 80	0.6467	0.7	0.8	1.1	0.1321	1.7	1.0	2.0
80 - 100	0.6077	0.9	0.8	1.2	0.1362	2.0	1.0	2.2
100 - 120	0.5312	1.1	0.8	1.4	0.1385	2.4	1.0	2.6
120 - 150	0.5009	1.0	0.8	1.3	0.1395	2.3	1.0	2.5
150 - 200	0.4695	1.0	0.8	1.3	0.1426	2.2	1.0	2.4

TABLE XIX. The final neutron capture cross section ratios of ^{122}Te, ^{123}Te, ^{124}Te, ^{125}Te, and ^{126}Te relative to ^{197}Au together with the statistical and systematic uncertainties in (%) (Energy bins as used for the calculation of the Maxwellian averaged cross sections).

Energy [keV]	$\sigma(^{122}Te)/\sigma(^{197}Au)$	uncertainty stat	sys	tot	$\sigma(^{123}Te)/\sigma(^{197}Au)$	uncertainty stat	sys	tot	$\sigma(^{124}Te)/\sigma(^{197}Au)$	uncertainty stat	sys	tot
5 - 7.5	0.3846	8.0	0.8	8.0	-	-	-	-	0.1966	11.1	0.8	11.1
7.5 - 10	0.4461	5.3	0.8	5.4	-	-	-	-	0.2596	6.4	0.8	6.4
10 - 12.5	0.4179	3.1	0.8	3.2	-	-	-	-	0.1969	4.6	0.8	4.7
12.5 - 15	0.5711	2.3	0.8	2.4	-	-	-	-	0.2851	2.9	0.8	3.0
15 - 20	0.5996	1.3	0.8	1.5	1.4292	1.6	0.8	1.8	0.3167	1.6	0.8	1.8
20 - 25	0.5551	1.1	0.8	1.4	1.5767	1.2	0.8	1.4	0.2977	1.4	0.8	1.6
25 - 30	0.5239	0.9	0.8	1.2	1.5567	1.0	0.8	1.3	0.2758	1.2	0.8	1.4
30 - 40	0.5427	0.7	0.8	1.1	1.5575	0.8	0.8	1.1	0.2742	1.0	0.8	1.3
40 - 50	0.5589	0.7	0.8	1.1	1.6283	0.7	0.8	1.1	0.2772	1.0	0.8	1.3
50 - 60	0.5072	0.8	0.8	1.1	1.6214	0.8	0.8	1.1	0.2798	1.0	0.8	1.3
60 - 80	0.5325	0.7	0.8	1.1	1.5739	0.7	0.8	1.1	0.2599	0.9	0.8	1.2
80 - 100	0.5202	0.8	0.8	1.1	1.5608	0.8	0.8	1.1	0.2755	1.1	0.8	1.4
100 - 120	0.5136	1.0	0.8	1.3	1.4695	1.1	0.8	1.4	0.2763	1.3	0.8	1.5
120 - 150	0.5232	0.9	0.8	1.2	1.4706	1.0	0.8	1.3	0.2730	1.2	0.8	1.4
150 - 175	0.5369	1.0	0.8	1.3	1.4035	1.1	0.8	1.4	0.2904	1.3	0.8	1.5
175 - 200	0.5621	1.2	0.8	1.4	1.2607	1.3	0.8	1.5	0.2879	1.5	0.8	1.7

Energy [keV]	$(^{125}Te)/\sigma(^{197}Au)$	uncertainty stat	sys	tot	$\sigma(^{126}Te)/\sigma(^{197}Au)$	uncertainty stat	sys	tot
5 - 7.5	-	-	-	-	0.1210	17.1	1.0	17.1
7.5 - 10	-	-	-	-	0.1218	13.2	1.0	13.2
10 - 12.5	-	-	-	-	0.1603	5.3	1.0	5.4
12.5 - 15	-	-	-	-	0.1531	5.0	1.0	5.1
15 - 20	0.8850	1.4	0.8	1.6	0.2174	2.4	1.0	2.6
20 - 25	1.0192	1.1	0.8	1.4	0.1522	2.6	1.0	2.8
25 - 30	0.9338	0.9	0.8	1.2	0.1448	2.2	1.0	2.4
30 - 40	0.8681	0.7	0.8	1.1	0.1356	1.8	1.0	2.1
40 - 50	0.8673	0.7	0.8	1.1	0.1412	1.8	1.0	2.1
50 - 60	0.7440	0.7	0.8	1.1	0.1500	1.8	1.0	2.1
60 - 80	0.6467	0.7	0.8	1.1	0.1321	1.7	1.0	2.0
80 - 100	0.6077	0.9	0.8	1.2	0.1362	2.0	1.0	2.2
100 - 120	0.5312	1.1	0.8	1.4	0.1385	2.4	1.0	2.6
120 - 150	0.5009	1.0	0.8	1.3	0.1395	2.3	1.0	2.5
150 - 175	0.4707	1.2	0.8	1.4	0.1405	2.4	1.0	2.6
175 - 200	0.4687	1.4	0.8	1.6	0.1455	2.6	1.0	2.8

TABLE XX. The neutron capture cross section of ^{122}Te, ^{123}Te, ^{124}Te, ^{125}Te, and ^{126}Te calculated from the experimental ratios using the gold data from literature [22,23].

Energy [keV]	$\sigma(^{197}Au)$ [mbarn]	$\sigma(^{122}Te)$ [mbarn]	$\sigma(^{123}Te)$ [mbarn]	$\sigma(^{124}Te)$ [mbarn]	$\sigma(^{125}Te)$ [mbarn]	$\sigma(^{126}Te)$ [mbarn]
5 - 10	1471.2	624.2	-	350.3	-	179.0
10 - 15	972.3	491.1	-	240.1	-	151.4
15 - 20	738.8	443.0	1055.9	234.0	653.8	160.6
20 - 30	585.4	314.0	916.5	166.7	567.0	86.3
30 - 40	500.4	271.6	779.4	137.2	434.4	67.9
40 - 60	411.5	218.8	668.4	114.6	329.7	60.0
60 - 80	349.4	186.1	549.9	90.8	226.0	46.2
80 - 100	298.3	155.2	465.6	82.2	181.3	40.6
100 - 120	290.1	149.0	426.3	80.2	154.1	40.2
120 - 150	274.1	143.4	403.1	74.8	137.3	38.2
150 - 200	258.1	141.4	345.6	74.7	121.2	36.8
5 - 7.5	1726.7	664.1	-	339.5	-	209.0
7.5 - 10	1215.7	542.3	-	315.6	-	148.1
10 - 12.5	1066.7	445.8	-	210.1	-	171.0
12.5 - 15	878.0	501.4	-	250.4	-	134.4
15 - 20	738.8	443.0	1055.9	234.0	653.8	160.6
20 - 25	600.0	333.1	946.1	178.6	611.5	91.3
25 - 30	570.8	299.0	888.6	157.5	533.1	82.7
30 - 40	500.4	271.6	779.4	137.2	434.4	67.9
40 - 50	433.3	242.2	705.6	120.1	375.8	61.2
50 - 60	389.6	197.6	631.7	109.0	289.9	58.5
60 - 80	349.4	186.1	549.9	90.8	226.0	46.2
80 - 100	298.3	155.2	465.6	82.2	181.3	40.6
100 - 120	290.1	149.0	426.3	80.2	154.1	40.2
120 - 150	274.1	143.4	403.2	74.8	137.3	38.2
150 - 175	263.7	141.5	370.0	76.6	124.1	37.1
175 - 200	252.6	142.0	318.4	72.7	118.4	36.8

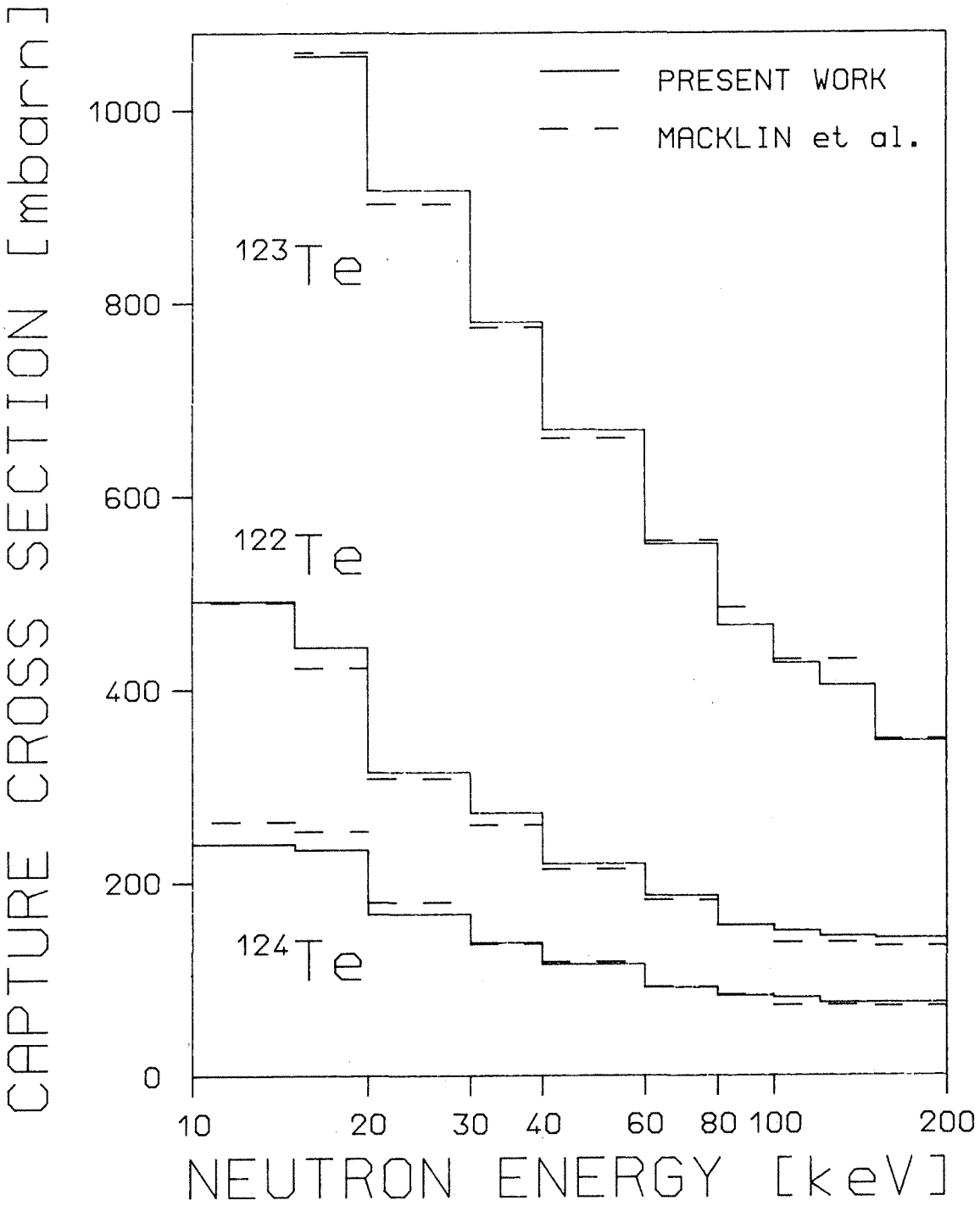

Fig. 10 The neutron capture cross section of the s-only tellurium isotopes in the energy range from 10 to 200 keV in comparison with the data of Macklin and Winters[7].

At 100 keV, the present data are lower by ~2 % while they are higher by ~4 % at 20 keV. An exception is ^{126}Te, where the cross section found in the present experiment is systematically lower by ~15 %. In view of this general good agreement, the comparison to the older data of Bergman and Romanov[24] and Macklin and Gibbons[25] can be taken from Ref. 7.

V. DISCUSSION OF UNCERTAINTIES

The determination of statistical and systematic uncertainties of the present experimental method has been described in Ref. 10. In the following we consider mainly new aspects that were inherent to the present experiment on the tellurium isotopes. The individual uncertainties are compiled in Table XXI.

(i) *Background subtraction.* The subtraction of the background due to sample scattered neutrons in the odd tellurium isotopes as described in Sec. III may lead to systematic uncertainties in the very low neutron energy range. There, the signal to background ratio is poor and the accuracy of the peak area around 6.9 MeV due to capture in ^{134}Ba and ^{136}Ba is not sufficient for a reliable background subtraction. For this reason, we hesitated to evaluate the data below 15 keV . The correlated uncertainty in the energy range above 15 keV was estimated to be well below the statistical uncertainty and was therefore neglected. This is confirmed by the fact that for ^{123}Te no systematic deviations from the data of Macklin and Winters[7] are observed at low neutron energies (see Fig. 10). In case of ^{125}Te the situation is not so clear. For this isotope, the shape is slightly different up to 100 keV, which can certainly not be explained by this effect.

(ii) *Flight path.* The flight path was measured several times during the experiment and was found reproducible within an accuracy of ±0.1 mm. In spite of the fact that the thickness of the samples varied between 0.8 and 5 mm, the mean flight path of the samples agreed within ±0.1 mm. Therefore, the uncertainty of 0.1 % quoted in Ref. 10 was found to be a reasonable estimate for the present experiment, too.

(iii) *Sample mass.* The uncertainty in the sample mass is dominated by the accuracy of the oxygen content, which is ±0.04 % in case of samples with low contamination (see Table II) and ±0.1 % for ^{123}Te. These results were confirmed in repeated measurements, and are, therefore, representative for the powder material. The final samples were prepared and

TABLE XXI. Systematic uncertainties [%].

Flight path (cross section ratio):		0.1
Neutron flux normalization (cross section ratio):		0.2
Sample mass (tellurium isotopes):		0.1
Isotopic enrichment (tellurium isotopes):		0.2
Multiple scattering (Au):		0.3
	(^{122}Te):	0.3
	(^{123}Te):	0.2
	(^{124}Te):	0.3
	(^{125}Te):	0.3
	(^{126}Te):	0.7
Unobserved events (cross section ratio):		0.6
total	$\sigma(^{122}Te)/\sigma(Au)$:	0.8
systematic	$\sigma(^{123}Te)/\sigma(Au)$:	0.8
uncertainties:	$\sigma(^{124}Te)/\sigma(Au)$:	0.8
	$\sigma(^{125}Te)/\sigma(Au)$:	0.8
	$\sigma(^{126}Te)/\sigma(Au)$:	1.0

weighed at the same time when the oxygen content was determined to make sure that no changes in stoechiometry took place. Actually, the weight of the samples increased in the time between preparation and canning by 0.2 mg in spite of the fact that they were always kept in an argon atmosphere. After cannig in a thin polyethylene foil, the weight increased during the seven month of the measurement by 0.6 - 1.7 mg/sample corresponding to less than 1 ‰ of the weight. Again, the situation was different for the ^{123}Te sample that showed an increase of 3 %. The additional mass is supposed to be due to further absorption of oxygen. While this does not affect the uncertainty of the mass determination, it increased the uncertainty of the multiple scattering correction (see below).

Impurities by other elements in the sample material were analysed by the suppliers and found to be below the detection limits between 0.05 % and 0.005 %. It is not expected

that these impurities can affect the sample mass beyond the uncertainty of 0.1 % given in Table XXI.

(iv) *Isotopic enrichment.* In the measurement of the isotopic composition performed at KfK, abundances of 5 % could be determined with an uncertainty of ≦1 % and abundances of 0.5 % with an uncertainty of ≦3 %. From these values, an uncertainty of 2 % can be interpolated for contributions to the isotopic pattern of 2 %. This percentage can be taken as a typical abundance of the isotopic impurities (Table III). Since the samples are enriched to 90 % or more, the 10 % impurities were determined with an average uncertainty of 2 %. This leads to an uncertainty of 0.2 % for the main isotope which was taken as the systematic uncertainty. This is a reasonable estimate according to the differences between our results and those of the suppliers.

The only remarkable discrepancy is the ^{123}Te content of the ^{122}Te sample, where a difference of 0.6 % was found. The sum of the isotopes 122 and 123, however, agrees to better than 1 ‰ . This leads to the idea that a limited mass resolution prevented a complete separation of the weak intensity of isotope 123 from the strong 122 component in one of the measurements. The mass separators used at KfK have a mass resolution of 500. It implies that for a mass around 100 the full width at tenth of the maximum of a peak in the mass spectrum is a factor of five smaller than the distance to the next isotope. Thus an incomplete mass separation can be excluded in our analysis and our data were assumed to be correct.

(v) *Isotopic correction.* The uncertainty discussed above causes an uncertainty in the number of atoms in the sample m(X) (see equ. 1). An additional uncertainty comes from the fact that part of the count rate Z_I is removed to account for the other isotopes as described in Sec. III. Fortunately, in the present experiment this correction is small. For the even isotopes it is dominated by the impurities of odd isotopes as they have larger cross sections. But as they have higher binding energies, too, the spectrum is changed essentially in the sum energy region around 9 MeV that is not used for the evaluation of the even isotopes at all. In contrary, the correction for the odd isotopes is small since the even isotopes, which dominate the impurities, have significantly smaller cross sections. In the TOF spectra (see e.g. Fig. 4) used for the determination of the cross section shape, the reduction in count rate by the isotopic correction was only 1-2 % with maximum values of ~4 % for the ^{124}Te sample. This correction is known with a systematic uncertainty of 2 %. This yields a final uncertainty less than 1‰ which was neglected.

The corrections (iv) and (v) are partly compensating each other, the combined effect being smaller as if they are treated independently. Thus even the 0.6 % discrepancy in the ^{123}Te content of the ^{122}Te sample would not change the final cross section by more than 0.4 %.

(vi) *Dead time and pile up.* Systematic uncertainties correlated with these effects were discussed in Ref. 10 and were found to be negligible.

(vii) *Normalization to equal neutron flux.* In the present experiment only the count rate of the neutron monitor close to the neutron target was used for normalization. Therefore, we slightly increased the corresponding uncertainty for the cross section ratio to 0.2 %. This seems rather conservative since the correction factors itself are of the order of 0.3 % only e.g., in run II. In Fig. 11, the normalization factors are plotted for the three runs dividing the data into three parts each. While in runs I and III where thin lithium targets were used a sizable correction is observed, the three times thicker target in run II caused nearly no correction. The scatter of the data points demonstrates that the assumed uncertainty of 0.2 % is a reasonable estimate.

(viii) *Spectrum fraction.* The systematic uncertainty of the fraction of unobserved capture events F_1 (see equation 1) was discussed in detail in Ref. 10, where a systematic uncertainty of 0.6 % was found. This discussion is still valid for the present experiment but part of the uncertainties are not relevant for the tellurium isotopes and affect only the gold spectrum. All cascades up to multiplicity 6 were included in the calculations. The variation of the energy threshold between 0 and 100 keV is irrelevant for capture in ^{122,123,125}Te since no transitions below 100 keV are observed in the compound nucleus. Thus the quoted uncertainty of 0.6 % is still acceptable for the cross section ratio of the tellurium isotopes relative to the gold standard. In the final use of the data in our s-process studies (see Sec. VII) where only the cross section ratios $\sigma(^{122}\mathrm{Te})/\sigma(^{124}\mathrm{Te})$ and $\sigma(^{123}\mathrm{Te})/\sigma(^{124}\mathrm{Te})$ are important the uncertainty in the cross section ratio is even smaller because the uncertainty due to the gold spectrum cancels out.

In Fig. 12, the correction F_1 is plotted versus the difference in binding energy of the respective tellurium isotope and the gold standard. The results show that a linear dependence is well established within the quoted uncertainty of 0.6 %. This could be expected since the shape of the sum energy spectra of the tellurium samples is very similar (see Fig. 5). More surprising is the fact that the relation crosses the zero point since the gold spectrum is

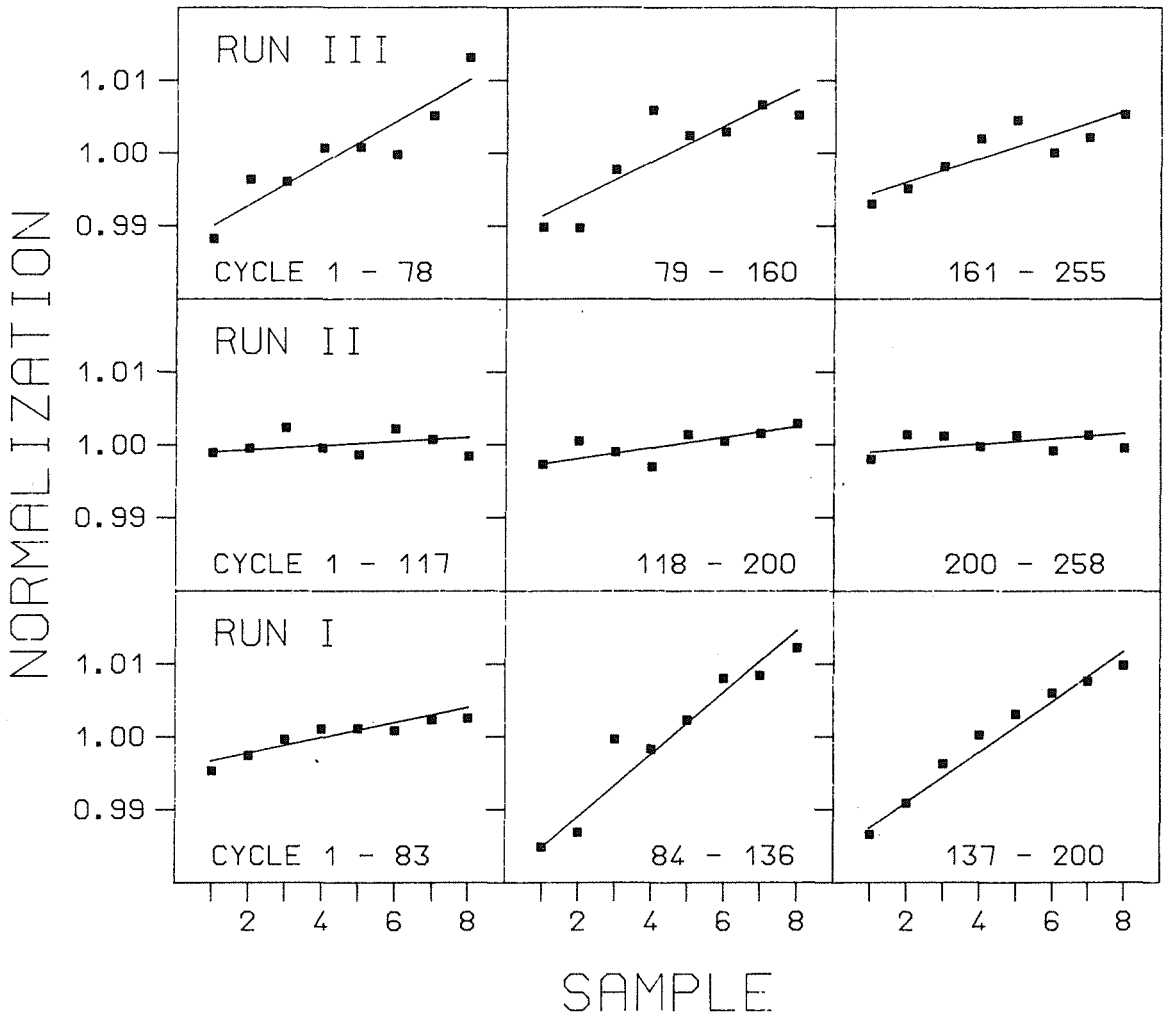

Fig. 11 Correction factors for normalization of the measured spectra to equal neutron fluence per sample. The data of each run were divided into three parts.

significantly different in shape. The figure documents that the derived uncertainty is a reasonable estimate.

The calculation of the fraction of unobserved capture events was checked by evaluating run I for a threshold in the sum energy of 1.9 MeV and 2.4 MeV. This difference affects only the normalization factor N and F_1 (see Eqs. 1 and 2), but their product should remain unchanged. The respective values are given in Table XXII. Both evaluations differ on average by ~1 %, but this difference can fully be explained by the statistical uncertainty of N and the systematic uncertainty of F_1. A larger systematic uncertainty in F_1 should show up immediately for the odd isotopes for which the correction is a factor of ten larger than for the even

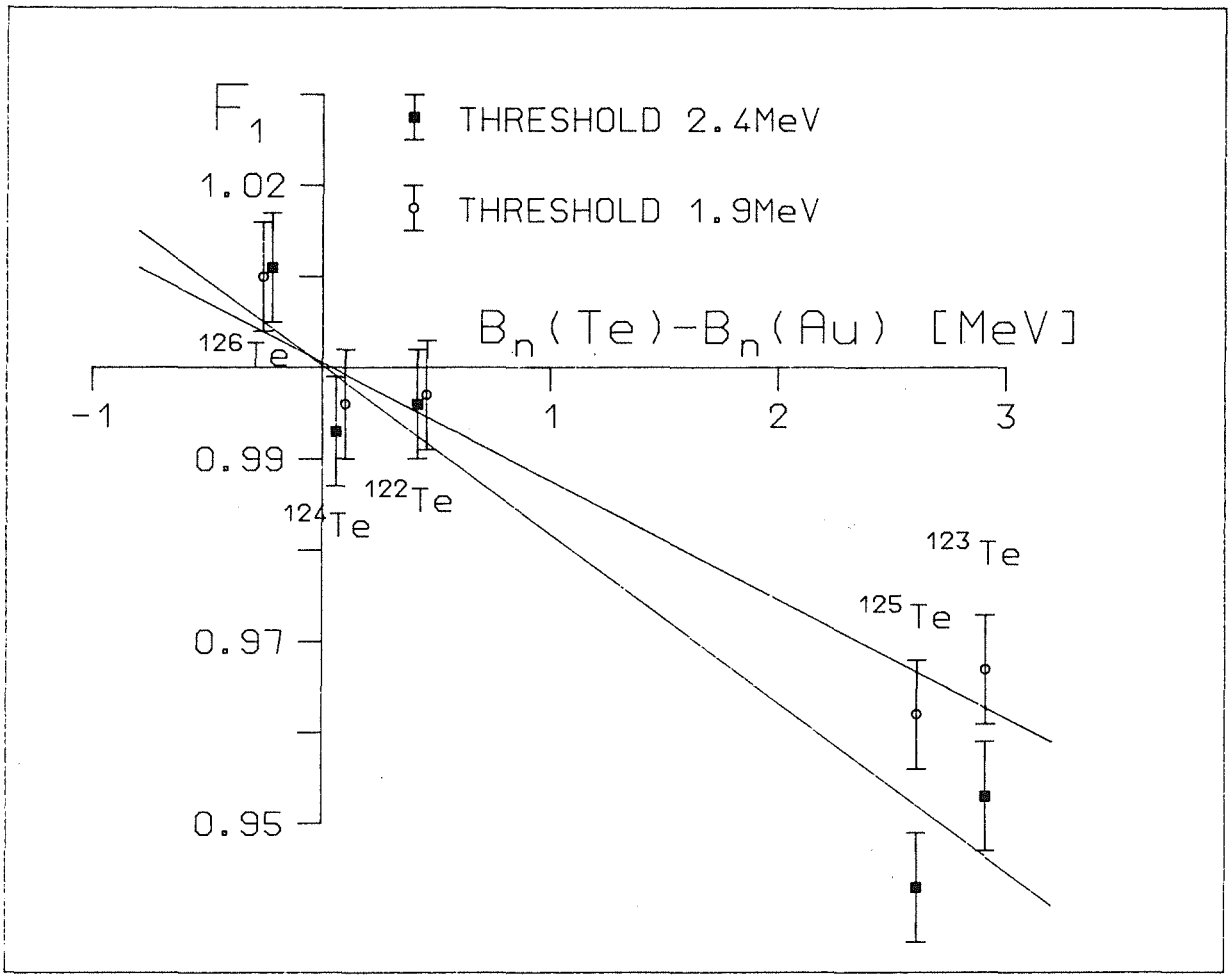

Fig. 12 The correction F_1 for unobserved capture events, plotted versus the difference in binding energy between Te isotope and gold standard.

isotopes. In our final results given in Tables XIII to XVII the higher threshold was used in run I, too, since the statistical uncertainty is smaller for that choice.

(ix) *Multiple scattering.* The multiple scattering and self shielding correction was calculated with different input parameters to study the systematic uncertainties. It turned out that this correction is most sensitive to the total cross section. For the odd isotopes the size of the correction is generaly small, because of the small sample mass and because multiple scattering and self-shielding compensate each other. The effect of the total cross section is much larger for the even isotopes. Especially the small capture cross section of ^{126}Te and the large sample mass had the consequence that MS is strongly dependent on the total cross section. The uncertainties given in Table XXI were derived from the assumption that the total cross section was reproduced within ±5 % in the calculation.

TABLE XXII. The product $N \times F_1$ (see Eqs. 1 and 2) evaluated for run I and two different thresholds in the sum-energy spectrum.

Cross section ratio	N	ΔN [%]	F_1	ΔF_1 [%]	$N \times F_1$	$\frac{N \times F_1(2.4\ MeV)}{N \times F_1(1.9\ MeV)}$
Threshold 1.9 MeV						
^{122}Te/Au	0.6945	1.2	0.9972	0.6	0.6926	1.010
^{123}Te/Au	2.1008	1.1	0.9672	0.6	2.0319	1.017
^{124}Te/Au	0.3810	1.8	0.9970	0.6	0.3798	1.007
^{125}Te/Au	0.8576	1.1	0.9623	0.6	0.8252	1.005
^{126}Te/Au	0.2079	3.7	1.0095	0.6	0.2099	1.021
Threshold 2.4 MeV						
^{122}Te/Au	0.7026	1.1	0.9957	0.6	0.6996	
^{123}Te/Au	2.1701	1.0	0.9527	0.6	2.0675	
^{124}Te/Au	0.3851	1.6	0.9934	0.6	0.3825	
^{125}Te/Au	0.8793	1.0	0.9431	0.6	0.8293	
^{126}Te/Au	0.2119	3.2	1.0118	0.6	0.2144	

The oxygen content had to be considered in the systematic uncertainty, too. The calculations for the ^{123}Te sample showed that a contamination of 12 % changes the correction by 0.008 on average. This result was used to estimate the systematic uncertainties caused by neglecting the initial oxygen content of all samples except for ^{123}Te and by the increase in mass observed during the experiment.

These estimates of the systematic uncertainties are correct for most of the energy range covered, but it seems somewhat optimistic for the values derived for ^{124}Te and ^{126}Te at 10 keV . The assumption on the total cross sections of ^{125,126}Te that were mainly based on the systematics of the other isotopes may also be critizised. But with the information given in Tables IX and XI it should be possible to derive revised values for this correction if new data for the total cross sections become available that differ significantly from the adopted ones.

VI. MAXWELLIAN AVERAGED CROSS SECTIONS

The Maxwellian averaged cross sections were calculated in the same way as described in Refs. 10 and 26. The neutron energy range from 0 to 600 keV was divided into four parts according to the cross sections from different sources. The respective contributions are tabulated in Tables XXIII to XXVII. The values I_3 were calculated using the cross sections of the present experiment in the fine energy binning given in the lower part of Table XX which is fine enough to make the correlated systematic uncertainty negligible. For the three s-only isotopes ^{122,123,124}Te, I_1 had to be calculated from resonance parameters[19] only in the interval from 0 to 1 keV. For part I_2 we used the data of Xia et al.[21] that were normalized to the present data in the overlapping energy range. The normalization factors as well as values derived for the cross section are given in Table XXVIII. This procedure was applicable since the cross section shapes were practically identical. The energy interval from 200 to 600 keV, that contributes only very little to the Maxwellian average at typical s-process temperatures was covered by the data of Macklin and Winters[7] normalized in the same way. The respective normalization factors calculated in the energy interval from 20 to 100 keV are given the lower part of Table XXVIII. For the isotopes ^{125,126}Te the data of Rev. 7 had to be used in the low energy range, too, and I_1 was extended from 0 to 3 keV .

The values δI_x given in Tables XXIII to XXVII are the statistical uncertainties for each of the parts. For the contribution derived from resonance parameters we assumed δI_1=10 %. The uncertainties δI_2 were calculated from the statistical uncertainties of the data of Xia et al.[21] and the statistical uncertainties of the normalization factors (see Table XXVIII). The later are small since the statistical uncertainties of the data of Ref. 21 is ~0.3 % in the overlapping energy range from 10 to 60 keV , almost negligible compared to the uncertainties of the present experiment (see Table XVIII). The uncertainties δI_4 were derived in the same way using the data of Ref. 7 and a normalizing interval from 20 to 100 keV. Since the statistical uncertainties were not specified in Ref. 7, an uncertainty of 1 % was assumed for each energy bin.

The systematic uncertainty of the Maxwellian averaged cross section given in Tables XXIII to XXVII is the uncertainty of the cross section ratio (see Table XXI) which has to be assigned to the summed intensity $I_2+I_3+I_4$. The 1.5 % uncertainty of the gold standard was not included since it cancels out in most applications of relevance for s-process studies (see Sec. VII). The total uncertainty is given in the last column. For temperatures in excess of kT=20 keV it is dominated by the systematic uncertainty.

TABLE XXIII. Maxwellian averaged neutron capture cross sections of ^{122}Te. The individual contributions I_x from different energy ranges ΔE are quoted separately together with their statistical uncertainties δI_x.

ΔE:	0 - 1 keV		1 - 10 keV		10 - 200 keV		200 - 600 keV		Total			
Data:	Resonance Parameter		from Xia et al.[21] (normalized)		Present Experiment		from Macklin [7] (normalized)					
kT [keV]	I_1 [mbarn]	δI_1	I_2 [mbarn]	δI_2	I_3 [mbarn]	δI_3	I_4 [mbarn]	δI_4	$\langle\sigma\rangle$ [mbarn]	$\delta\langle\sigma\rangle$ stat.	syst.[a]	total
10	25.7	2.6	215.9	2.7	299.5	2.6	0.0	0.0	541.1	4.6	4.1	6.2
12	18.0	1.8	164.4	2.0	306.3	2.4	0.0	0.0	488.7	3.6	3.8	5.2
20	6.6	0.7	71.6	0.8	289.7	1.9	0.0	0.0	367.9	2.2	2.9	3.6
25	4.3	0.4	48.5	0.5	272.5	1.6	0.3	0.0	325.6	1.7	2.6	3.1
30	3.0	0.3	35.0	0.4	256.3	1.4	1.1	0.0	295.4	1.5	2.3	2.7
40	1.7	0.2	20.7	0.2	227.6	1.2	5.2	0.1	255.2	1.2	2.0	2.3
50	1.1	0.1	13.7	0.1	202.9	1.1	12.7	0.1	230.3	1.1	1.8	2.1
52	1.0	0.1	12.7	0.1	198.3	1.0	14.5	0.2	226.4	1.0	1.8	2.1
60	0.8	0.1	9.7	0.1	181.0	0.9	22.2	0.2	213.6	0.9	1.7	1.9
70	0.6	0.1	7.2	0.1	161.7	0.9	32.4	0.3	201.8	1.0	1.6	1.9
80	0.4	0.0	5.6	0.1	144.8	0.8	42.3	0.4	193.1	0.9	1.5	1.7
90	0.3	0.0	4.4	0.1	129.9	0.7	51.4	0.5	186.0	0.9	1.5	1.7
100	0.3	0.0	3.6	0.0	117.0	0.6	59.3	0.5	180.2	0.8	1.4	1.6

[a] The uncertainty of 1.5 % of the gold standard is not included in the systematic uncertainty since it cancels out in most applications of relevance for nuclear astrophysics (see Sec. VII).

TABLE XXIV. Maxwellian averaged neutron capture cross sections of ^{123}Te. The individual contributions I_x from different energy ranges ΔE are quoted separately together with their statistical uncertainties δI_x.

ΔE:	0 - 1 keV		1 - 15 keV		15 - 200 keV		200 - 600 keV		Total			
Data:	Resonance Parameter		from Xia et al.[21] (normalized)		Present Experiment		from Macklin [7] (normalized)					
kT [keV]	I_1 [mbarn]	δI_1	I_2 [mbarn]	δI_2	I_3 [mbarn]	δI_3	I_4 [mbarn]	δI_4	$\langle\sigma\rangle$ [mbarn]	$\delta\langle\sigma\rangle$ stat.	syst.[a]	total
10	33.7	3.4	848.4	11.0	554.0	4.3	0.0	0.0	1436.1	12.3	11.2	16.6
12	23.6	2.4	669.3	8.1	617.4	4.4	0.0	0.0	1310.3	9.5	10.3	14.0
20	8.6	0.9	314.8	3.4	693.7	4.2	0.1	0.0	1017.2	5.5	8.1	9.8
25	5.6	0.6	219.0	2.3	685.7	3.9	0.6	0.0	910.8	4.6	7.2	8.5
30	3.9	0.4	160.9	1.6	664.6	3.6	2.1	0.0	831.5	4.0	6.6	7.7
40	2.2	0.2	97.2	1.0	609.3	3.2	10.2	0.1	718.9	3.4	5.7	6.6
50	1.4	0.1	64.9	0.6	550.3	2.8	24.5	0.3	641.2	2.9	5.1	5.9
52	1.3	0.1	60.4	0.6	538.6	2.8	27.9	0.3	628.2	2.9	5.0	5.8
60	1.0	0.1	46.4	0.5	493.7	2.6	42.3	0.4	583.4	2.7	4.7	5.4
70	0.7	0.1	34.8	0.3	442.0	2.3	60.8	0.6	538.3	2.4	4.3	4.9
80	0.6	0.1	27.1	0.3	395.9	2.1	78.1	0.7	501.7	2.2	4.0	4.6
90	0.4	0.0	21.7	0.2	355.3	1.9	93.5	0.8	470.9	2.1	3.8	4.3
100	0.4	0.0	17.7	0.2	319.8	1.7	106.4	0.9	444.3	1.9	3.6	4.1

[a] The uncertainty of 1.5 % of the gold standard is not included in the systematic uncertainty as it cancels out in most applications of relevance for nuclear astrophysics (see Sec. VII).

TABLE XXV. Maxwellian averaged neutron capture cross sections of ^{124}Te. The individual contributions I_x from different energy ranges ΔE are quoted separately together with their statistical uncertainties δI_x.

ΔE:	0 - 1 keV		1 - 10 keV		10 - 200 keV		200 - 600 keV		Total			
Data:	Resonance Parameter		from Xia et al.[21] (normalized)		Present Experiment		from Macklin [7] (normalized)					
kT [keV]	I_1 [mbarn]	δI_1	I_2 [mbarn]	δI_2	I_3 [mbarn]	δI_3	I_4 [mbarn]	δI_4	$\langle\sigma\rangle$ [mbarn]	$\delta\langle\sigma\rangle$ stat.	syst.[a]	total
10	6.8	0.7	128.7	1.7	153.3	1.8	0.0	0.0	288.8	2.6	2.3	3.5
12	4.8	0.5	98.0	1.3	157.1	1.7	0.0	0.0	259.9	2.2	2.0	3.0
20	3.1	0.3	42.6	0.5	148.9	1.3	0.0	0.0	194.6	1.4	1.5	2.1
25	1.8	0.2	28.9	0.3	140.2	1.1	0.2	0.0	171.0	1.2	1.4	1.8
30	1.1	0.1	20.8	0.2	132.0	1.0	0.6	0.0	154.6	1.0	1.2	1.6
40	0.8	0.1	12.3	0.1	117.5	0.9	2.7	0.0	133.3	0.9	1.1	1.4
50	0.6	0.1	8.1	0.1	105.0	0.8	6.7	0.1	120.4	0.8	1.0	1.3
52	0.5	0.1	7.5	0.1	102.6	0.7	7.6	0.1	118.2	0.7	0.9	1.1
60	0.3	0.0	5.7	0.1	93.8	0.7	11.7	0.1	111.5	0.7	0.9	1.1
70	0.3	0.0	4.3	0.1	83.9	0.6	17.1	0.2	105.6	0.6	0.8	1.0
80	0.2	0.0	3.3	0.0	75.2	0.6	22.3	0.2	101.0	0.6	0.8	1.0
90	0.2	0.0	2.6	0.0	67.6	0.5	27.1	0.2	97.5	0.5	0.8	0.9
100	0.1	0.0	2.2	0.0	60.9	0.5	31.3	0.3	94.5	0.6	0.8	1.0

[a] The uncertainty of 1.5 % of the gold standard is not included in the systematic uncertainty since it cancels out in most applications of relevance for nuclear astrophysics (see Sec. VII).

TABLE XXVI. Maxwellian averaged neutron capture cross sections of ^{125}Te. The individual contributions I_x from different energy ranges ΔE are quoted separately together with their statistical uncertainties δI_x.

ΔE:	0 - 3 keV		3 - 15 keV		15 - 200 keV		200 - 600 keV		Total			
Data:	Resonance Parameter		from Macklin[7] (normalized)		Present Experiment		from Macklin[7] (normalized)					
kT [keV]	I_1 [mbarn]	δI_1	I_2 [mbarn]	δI_2	I_3 [mbarn]	δI_3	I_4 [mbarn]	δI_4	$\langle\sigma\rangle$ [mbarn]	$\delta\langle\sigma\rangle$ stat.	syst.[a]	total
10	83.3	8.3	400.9	3.1	331.0	2.4	0.0	0.0	815.2	9.2	5.9	10.9
12	59.4	5.9	323.2	2.6	362.4	2.4	0.0	0.0	745.0	6.9	5.5	8.8
20	22.6	2.2	158.2	1.3	379.6	2.2	0.0	0.0	560.4	3.4	4.3	5.5
25	14.7	1.5	111.2	0.9	360.7	2.0	0.2	0.0	486.8	2.7	3.8	4.7
30	10.3	1.0	82.3	0.7	337.7	1.8	0.9	0.0	431.2	2.2	3.4	4.0
40	5.9	0.6	50.2	0.4	293.0	1.5	4.4	0.1	353.4	1.7	2.8	3.3
50	3.8	0.4	33.7	0.3	254.2	1.3	10.5	0.1	302.2	1.4	2.4	2.8
52	3.5	0.4	31.4	0.3	247.2	1.1	12.0	0.1	294.1	1.2	2.3	2.6
60	2.7	0.3	24.2	0.2	221.6	1.0	18.2	0.2	266.6	1.1	2.1	2.4
70	2.0	0.2	18.2	0.2	194.2	1.0	26.2	0.3	240.5	1.1	1.9	2.2
80	1.5	0.2	14.2	0.1	171.1	0.9	33.8	0.3	220.6	1.0	1.8	2.1
90	1.2	0.1	11.3	0.1	151.6	0.8	40.5	0.4	204.6	0.9	1.6	1.8
100	1.0	0.1	9.3	0.1	135.0	0.7	46.2	0.4	191.4	0.8	1.5	1.7

[a] The uncertainty of 1.5 % of the gold standard is not included in the systematic uncertainty since it cancels out in most applications of relevance for nuclear astrophysics (see Sec. VII).

TABLE XXVII. Maxwellian averaged neutron capture cross sections of ^{126}Te. The individual contributions I_x from different energy ranges ΔE are quoted separately together with their statistical uncertainties δI_x.

ΔE:	0 - 3 keV		3 - 10 keV		10 - 200 keV		200 - 600 keV		Total			
Data:	Resonance Parameter		from Macklin[7] (normalized)		Present Experiment		from Macklin[7] (normalized)					
kT [keV]	I_1 [mbarn]	δI_1	I_2 [mbarn]	δI_2	I_3 [mbarn]	δI_3	I_4 [mbarn]	δI_4	$\langle\sigma\rangle$ [mbarn]	$\delta\langle\sigma\rangle$ stat.	syst.[a]	total
10	16.2	1.6	43.4	0.4	92.6	1.9	0.0	0.0	152.1	2.5	1.4	2.9
12	11.6	1.2	33.6	0.3	92.8	1.8	0.0	0.0	138.0	2.2	1.3	2.6
20	4.4	0.4	15.1	0.2	83.4	1.4	0.0	0.0	103.0	1.5	1.0	1.8
25	2.9	0.3	10.3	0.1	77.0	1.2	0.1	0.0	90.3	1.2	0.9	1.5
30	2.0	0.2	7.5	0.1	71.5	1.1	0.3	0.0	81.3	1.1	0.8	1.4
40	1.2	0.1	4.5	0.0	62.5	0.9	1.4	0.0	69.5	0.9	0.7	1.1
50	0.8	0.1	3.0	0.0	55.1	0.8	3.3	0.0	62.2	0.8	0.6	1.0
52	0.7	0.1	2.8	0.0	53.8	0.8	3.8	0.0	61.0	0.8	0.6	1.0
60	0.5	0.1	2.1	0.0	48.9	0.7	5.8	0.1	57.3	0.7	0.6	0.9
70	0.4	0.0	1.6	0.0	43.5	0.7	8.4	0.1	53.9	0.7	0.5	0.9
80	0.3	0.0	1.2	0.0	38.9	0.6	11.0	0.1	51.4	0.6	0.5	0.8
90	0.2	0.0	1.0	0.0	34.8	0.5	13.4	0.2	49.4	0.5	0.5	0.7
100	0.2	0.0	0.8	0.0	31.3	0.5	15.4	0.2	47.7	0.5	0.5	0.7

[a] The uncertainty of 1.5 % of the gold standard is not included in the systematic uncertainty since it cancels out in most applications of relevance for nuclear astrophysics (see Sec. VII).

TABLE XXVIII. Data from Xia et al.[21] and Macklin and Winters[7] used for the determination of Maxwellian averaged capture cross sections.

Energy range [keV]	σ(Te)/σ(Au)	Normalization factor	σ(Au) [mbarn]	σ(Te) [mbarn]
		Xia et al.[21]		
^{122}Te				
1 - 3	0.3282 ± 4.4 %	1.074 ± 0.5 %	4013.0	1317
3 - 5	0.3385 ± 1.9 %		2266.8	767
5 - 10	0.4107 ± 0.7 %		1471.2	604
^{123}Te				
1 - 3	1.0166 ± 5.9 %	1.061 ± 0.5 %	4013.0	4079.6
3 - 5	0.8739 ± 2.6 %		2266.8	1981.0
5 - 10	1.0973 ± 0.9 %		1471.2	1614.4
10 - 15	1.2985 ± 0.7 %		972.4	1262.7
^{124}Te				
1 - 3	0.1972 ± 4.4 %	1.004 ± 0.6 %		791.4
3 - 5	0.2096 ± 2.0 %			475.1
5 - 10	0.2405 ± 0.8 %			353.8

Macklin and Winters[7]

	σ(pres. exp.) / σ(Macklin)	⟨σ⟩(pres. exp.) / ⟨σ⟩(Macklin)	⟨σ⟩(pres. exp.) / ⟨σ⟩(Macklin)
Normalization interval:	20-100 keV	kT = 20-30 keV	kT = 10 keV
^{122}Te	1.026 ± 0.6 %	1.060	1.104
^{123}Te	0.999 ± 0.6 %	1.022	1.071
^{124}Te	0.981 ± 0.6 %	1.006	0.992
^{125}Te	1.013 ± 0.6 %	1.022	1.025
^{126}Te	0.856 ± 0.9 %	0.916	0.874

We note that in determining ratios, as e.g. $\langle\sigma\rangle(^{122}Te)/\langle\sigma\rangle(^{124}Te)$, it is not allowed to add the uncertainties given in Tables XIII and XV quadratically, because they are highly correlated. For example, the statistical uncertainties of the cross section ratios are partly determined by the count rate in the gold spectra ($Z_1(Au)$, $\Sigma Z(Au)$, $\Sigma E(Au)$ in Eq.1) which cancels out in the cross section ratio of two tellurium isotopes. The same holds for the systematic uncertainties for multiple scattering and for the spectrum fraction of the gold sample. The exact uncertainty of the ratio of Maxwellian averaged cross sections of two tellurium isotopes is complicated to determine and will be discussed in detail in Sec. VII. As an estimate, the larger value of the two cross sections involved in the ratio could be used, since statistical and systematic uncertainties of the gold sample and the tellurium samples are similar.

The present results are compared with the data of Macklin and Winters[7] in the last two columns of Table XXVIII. If the values for kT=20-30 keV are compared with the normalization factors in column 1, one finds that our Maxwellian averages are about 2 % higher for the isotopes $^{123,124,125}Te$. A little bit surprising is the result for ^{122}Te, where a 6 % difference is obtained though the cross section in the range from 3 to 10 keV of Xia et al.[21] is quite similar to the data of Macklin and Winters[7]. This effect is even more pronounced at kT=10 keV. The largest differences are observed for ^{126}Te. For this isotope the uncertainty claimed by Macklin and Winters[7] it is hard to understand because the same sample mass was used for ^{126}Te and ^{123}Te. Since the capture cross sections of the two isotopes differ by a factor of 10, a much larger correction for scattered neutrons and, therefore, a larger uncertainty would be expected for ^{126}Te.

VII. IMPLICATIONS FOR THE CLASSICAL s-PROCESS AND FOR STELLAR MODELS

The classical concept of the s-process dates back to the basic paper by Burbidge et al.[27] and simply assumes the irradiation of a certain fraction G of the observed ^{56}Fe abundance by a suited neutron exposure. This approach has been detailed by Seeger, Fowler, and Clayton[28], who showed that the observed s-process abundances can be described by means of an exponential distribution of neutron exposures τ,

$$\rho(\tau) = \frac{G\, N_{\odot}^{56}}{\tau_o} \exp(-\tau/\tau_o) \,, \qquad (3)$$

τ being the time integrated neutron flux.

This assumption on the type of neutron exposure is characterized by only two parameters, the fraction G of the observed ^{56}Fe abundance and the mean neutron exposure, τ_o; it allows one to solve analytically the set of coupled differential equations describing the abundances of the entire neutron capture chain from iron to bismuth. However, this solution requires two simplifications, i.e., that the neutron density and the temperature are constant throughout the duration of the s-process. Then the product $\langle\sigma\rangle N_s$ of the stellar cross section, $\langle\sigma\rangle$, and the s-process abundance, N_s - which is the characteristic quantity describing the s-process flow - can be expressed as a function of mass number[29]:

$$\langle\sigma\rangle N_s(A) = \frac{G\, N_{\odot}^{56}}{\tau_o} \prod_{i=56}^{A} \left(1 + \frac{1}{\langle\sigma\rangle_i \tau_o} \right)^{-1} \qquad (4)$$

which depends only on the Maxwellian averaged neutron capture cross sections, $\langle\sigma\rangle_i$, along the neutron capture chain. The two parameters, G and τ_o, are determined by a least-squares fit of the $\langle\sigma\rangle N_s(A)$ curve to the empirical $\langle\sigma\rangle N_s$ values of those nuclei, which are produced exclusively by the s-process. A detailed description of the classical s-process approach is given in Refs. 1 and 30.

In deriving equation 4, it was additionally assumed that the neutron capture rates should be either much faster or much slower than the beta decay rates of the unstable isotopes produced. In other words, possible branchings of the neutron capture path due to competition between beta decays and neutron captures were neglected. The proper treatment of branchings in the framework of the classical approach was formulated by Ward, Newman, and Clayton[31] and is given in Ref.30. The strength of a branching can be described by the branching factor f_n or f_β (see Sec. I). In the following we use the the factor $f_\beta=\lambda_\beta/(\lambda_\beta+\lambda_n)$ instead of f_n in order to keep the formulas simpler.

The s-process path in the region of the tellurium isotopes is shown in Fig. 1. There are two possible branching points at the unstable isotopes ^{121}Sn and ^{122}Sb. The situation is complicated by the fact that neutron capture in ^{120}Sn may lead either to the ground state or the isomeric state in ^{121}Sn, that have to be treated independently[32]. The fraction of capture events to the isomer is defined as IR. In case of neutron capture in ^{121}Sb there is an isomeric state, too, but as both ground state and isomer have about the same half-life they can be treated as a single isotope. For this branching, however, one has to consider the possibility of β^+ decay or electron capture (EC) to ^{122}Sn, giving rise to a second branching factor $f_\beta{}^1=\lambda_{\beta^-}/(\lambda_{\beta^-} + \lambda_{EC,\beta^+} + \lambda_n)$. In this relation λ_{EC} and λ_{β^+} are the decay rates for the respective decays defined in the same way as the decay rate for β^- decay (see Sec. I).

Equation 4 can also be written as a recursive formula:

$$\langle\sigma\rangle N(^{A}Z) = \zeta(^{A}Z) \times \langle\sigma\rangle N(^{A-1}Z)\ , \tag{5a}$$

with the propagator

$$\zeta(^{A}Z) = \left(1 + \frac{1}{\tau_o \langle\sigma\rangle(^{A}Z)} \right)^{-1}. \tag{5b}$$

If ^{A}Z is a branch point, the propagator ζ has to be replaced by:

$$\xi(^{A}Z) = \left(\frac{1}{1 - f_\beta} + \frac{1}{\tau_o \langle\sigma\rangle(^{A}Z)} \right)^{-1}, \tag{6}$$

to calculate the $\langle\sigma\rangle N$-value in the neutron-rich part of the branching. The contribution to the isobar Z+1 via β^- decay is then given by:

$$\langle\sigma\rangle N(^{A}(Z+1)) = \frac{f_\beta}{1 - f_\beta}\ \zeta(^{A}(Z+1)) \times \langle\sigma\rangle N(^{A}Z). \tag{7}$$

The s-process path from ^{119}Sn to ^{124}Te is described by the following equations[32]:

$$\langle\sigma\rangle N(^{120}Sn) = \zeta(^{120}Sn) \times \langle\sigma\rangle N(^{119}Sn) \tag{8}$$

$$\langle\sigma\rangle N(^{121m}Sn) = IR \times \xi(^{121m}Sn) \times \langle\sigma\rangle N(^{120}Sn) \tag{9}$$

$$\langle\sigma\rangle N(^{122}Sn) = \zeta(^{122}Sn) \times \left(\langle\sigma\rangle N(^{121m}Sn) + \frac{f_\beta(^{122}Sb)}{1 - f_\beta(^{122}Sb)} (1 - f_\beta{}^{1}(^{122}Sb)) \times \langle\sigma\rangle N(^{122}Sb) \right) \tag{10}$$

$$\langle\sigma\rangle N(^{121}Sb) = \zeta(^{121}Sb) \times \left((1-IR) \times \langle\sigma\rangle N(^{120}Sn) + \frac{f_\beta(^{121}Sn)}{1 - f_\beta(^{121}Sn)} \times \langle\sigma\rangle N(^{121m}Sn) \right) \tag{11}$$

$$\langle\sigma\rangle N(^{122}Sb) = \xi(^{122}Sb) \times \langle\sigma\rangle N(^{121}Sb) \tag{12}$$

$$\langle\sigma\rangle N(^{123}Sb) = \zeta(^{123}Sb) \times (\langle\sigma\rangle N(^{122}Sn) + \langle\sigma\rangle N(^{122}Sb)) \tag{13}$$

$$\langle\sigma\rangle N(^{122}Te) = \zeta(^{122}Te) \times \frac{f_\beta(^{122}Sb)}{1 - f_\beta(^{122}Sb)} \times f_\beta{}^{1}(^{122}Sb) \times \langle\sigma\rangle N(^{122}Sb) \tag{14}$$

$$\langle\sigma\rangle N(^{123}Te) = \zeta(^{123}Te) \times \langle\sigma\rangle N(^{122}Te) \tag{15}$$

$$\langle\sigma\rangle N(^{124}Te) = \zeta(^{124}Te) \times (\langle\sigma\rangle N(^{123}Te) + \langle\sigma\rangle N(^{123}Sb)) \tag{16}$$

This set of equations was solved to determine the s-process abundances of the isotopes ^{122,123,124}Te which can then be compared to the abundances observed in the solar system. For this purpose a variety of input parameters are necessary:

Neutron capture cross sections: The neutron capture cross sections for the s-only isotopes were taken from the present investigation. Three of the other involved isotopes have recently be measured at KfK using the activation technique[32], the others were taken from literature[13,33,34]. The actual values are compiled in Table XXIX.

TABLE XXIX. Input data for the stellar neutron capture cross sections used in the calculations according to the classical model.

Isotope	<σ> (mbarn)*	Reference
^{116}Sn	93.6 ± 5	Beer et al. (Ref. 33)
^{117}Sn	409 ±78	Bao and Käppeler (Ref. 13)
^{118}Sn	64 ± 12	Bao and Käppeler
^{119}Sn	251 ± 48	Bao and Käppeler
^{120}Sn	32.5 ± 1.4	Schanz (Ref. 32)
^{121m}Sn	194	Holmes et al. (Ref. 34)
^{122}Sn	23 ± 5	Bao and Käppeler
^{121}Sb	541 ± 15	Schanz (Ref. 32)
^{123}Sb	309 ± 9	Schanz (Ref. 32)
^{122}Te	300.5 ± 2.7	present work
^{123}Te	845.7 ± 7.8	present work
^{124}Te	157.2 ± 1.6	present work

* Maxwellian averaged cross sections at kT = 29 keV, extrapolated according to 1/v from the data given for kT = 30 keV.

Neutron density and temperature: These parameters that are required to calculate λ_n and λ_β were adopted from an evaluation of all important branchings[30]:

$$n_n = (3.4 \pm 1.1) \times 10^8 \text{ cm}^{-3}$$

$$kT = 29 \pm 5 \text{ keV}, \qquad T = (3.3 \pm 0.5) \times 10^8 \text{ K}$$

Mean neutron irradiation: The isotopes under investigation are completely formed by the main component of the s-process flow, which is characterized by a mean neutron exposure[30]:

$$\tau_o = 0.295 \pm 0.009 \text{ mbarn}^{-1}.$$

Beta-decay rates: The beta decay rates of unstable isotopes may be drastically changed under stellar conditions. In the present investigation such an enhancement can be expected for the beta decay of ^{121}Sn. According to the calculations of Takahashi and Yokoi[35] the decay rate is increased by a factor 2.9 at a temperature of 3.3×10^8 K . This enhancement,

however, is valid only for a thermal equilibrium between ground state and isomer. As discussed in Ref. 32, that followed the procedure recommended by Klay et al.[36], thermal equilibrium is not reached in ^{121}Sn. This means that the isomeric state is quickly depopulated to the ground state, resulting in a stellar decay rate corresponding to the laboratory value. As a further consequence, the isomeric ratio IR reduces to zero in Eqs. 9 and 11.

With the parameters compiled above, the abundances N_s of the s-only isotopes ^{122,123,124}Te were calculated and the ratio $N_s/N_\odot$ to the solar abundances was determined. The results were normalized to the ^{124}Te abundance, since this isotope experiences the entire mass flow. This procedure allows to use the isotopic abundances given with an accuracy of about 1 ‰ in Ref. 6 (^{122}Te 2.603 (3), ^{123}Te 0.908 (1), and ^{124}Te 4.816 (3)). The results are compiled in Table XXX. For a perfect model, all values should be unity. Obviously, the classical approach comes very close to this ideal case. For the first time, the prediction of the classical model of the "local approximation" , i.e. that the product $\langle\sigma\rangle N_s$ is constant for neighboring isotopes, could be checked on the 1 % level for a set of three s-only isotopes. The neutron density of the classical model is sufficiently low, that the branchings at ^{121}Sn and ^{122}Sb are not yet activated. Within the experimental uncertainties, a very weak branching of at most ~1 % would be possible if one considers the $\langle\sigma\rangle N_s$-values of ^{123}Te and ^{124}Te only (for ^{122}Te see below). The corresponding upper limit for the neutron density:

$$n_n < 6.0 \times 10^8 \text{ cm}^{-3}$$

is well in agreement with the value quoted above.

The uncertainty of the predicted s-process abundances are completely dominated by the uncertainty of the ratios:

$\langle\sigma\rangle N_s(^{122}\text{Te})/\langle\sigma\rangle N_s(^{124}\text{Te})$ and $\langle\sigma\rangle N_s(^{123}\text{Te})/\langle\sigma\rangle N_s(^{124}\text{Te})$.

The abundances being known with a negligible uncertainty of 1 ‰ implies that the uncertainty is determined by the cross section ratio only. This uncertainty can not be calculated from the values given in Tables XXIII to XXV (see Sec. VI) since the uncertainties related to the gold sample cancel out in the ratio. Therefore, a thorough correlation analysis was performed yielding the uncertainties for the Maxwellian averaged cross section ratios that are given in Table XXXI.

The present results for the classical model allow also for a discussion of limits for the p-process abundances of the tellurium isotopes. There is agreement among current p-process models[37,38] that the odd isotope ^{123}Te is not produced in the high temperature regime

TABLE XXX. s-Process production ratios of ^{122}Te, ^{123}Te, and ^{124}Te relative to solar abundances (normalized at ^{124}Te).

Isotope	Classical model		Low mass stars	
	present work	Macklin*	present work	Macklin*
^{122}Te	0.984 ± 0.012	1.032 ± 0.057	0.91 ± 0.01**	0.96 ± 0.06**
^{123}Te	1.003 ± 0.012	1.021 ± 0.051	0.94 ± 0.01**	0.96 ± 0.05**
^{124}Te	1	1	1	1

* capture cross sections from Macklin and Winters[7]

** error bars due to uncertainty of the capture cross section of tellurium isotopes. An additional uncertainty of ~0.01 comes from the cross sections of the unstable isotopes ^{121}Sn and ^{122}Sb.

TABLE XXXI. The ratio of the Maxwellian averaged neutron capture cross sections of two tellurium isotopes and the correlated uncertainties.

kT	$\langle\sigma\rangle(^{122}Te)/\langle\sigma\rangle(^{124}Te)$	$\langle\sigma\rangle(^{123}Te)/\langle\sigma\rangle(^{124}Te)$
10	1.874 ± 1.5 %	4.973 ± 1.5 %
12	1.880 ± 1.4 %	5.042 ± 1.4 %
20	1.891 ± 1.3 %	5.227 ± 1.2 %
25	1.904 ± 1.2 %	5.326 ± 1.2 %
30	1.911 ± 1.2 %	5.378 ± 1.2 %
40	1.914 ± 1.2 %	5.393 ± 1.2 %
50	1.913 ± 1.2 %	5.326 ± 1.2 %
52	1.915 ± 1.2 %	5.315 ± 1.2 %
60	1.916 ± 1.2 %	5.232 ± 1.1 %
70	1.911 ± 1.1 %	5.098 ± 1.1 %
80	1.912 ± 1.1 %	4.967 ± 1.1 %
90	1.908 ± 1.1 %	4.830 ± 1.1 %
100	1.907 ± 1.1 %	4.702 ± 1.1 %

of the p-process. In this case, the equality of the $\langle\sigma\rangle N_s$-values of ^{123}Te and ^{124}Te has the consequence that the p-process contribution to ^{124}Te is also zero. Therefore, it is not possible that a weak branching may be compensated by p-process contributions to ^{122}Te and ^{123}Te. It has to be noted, that the tellurium isotopes provide for the only branching with three s–only nuclei including an odd isotope where such a test is possible. At face value, the abundance ratio of 0.984 derived for ^{122}Te could be interpreted as a 1.5 % p-process contribution. Given the experimental uncertainties , this is not a quantitative assignment, but it appears quite reasonable if it is compared to the abundance of the pure p-nucleus ^{120}Te, which is ~3 % of the ^{122}Te abundance.

The cross sections obtained in the present experiment were also used to calculate the s-process abundances in the Te region with a stellar model. At present, the most successful approach is the stellar helium burning in low mass stars (Gallino et al.[30,39]), that allows for a quantitative description of the abundance pattern of the main component. Adopting the profiles for neutron density, temperature, and mass density from this model[40], the s-process flow through the mass region 110<A<130 was followed with the network code NETZ[41]. Preliminary results are included in Table XXX, indicating that this model predicts significant branchings at A = 121,122, which cause ~ 6 % of the flow to bypass ^{122}Te and ^{123}Te. This is the consequence of the higher neutron density implied by the stellar model compared to the classical approach. A detailed discussion of this discrepancy and its astrophysical implications will be presented in a forthcoming publication[42].

The importance of using very accurate cross sections in these investigations is underlined, if the above s-process studies are repeated using respective data of Macklin and Winters[7]. In this case, the significant difference between the classical approach and the stellar model is completely masked by the larger uncertainties of ~5 %. Obviously, the new experimental technique allows for a much more detailed discussion of the information contained in the observed abundances, and, hence, represents a significant step towards a deeper understanding of the s-process and of the helium burning stages in stellar evolution.

VIII. CONCLUSIONS

A new experimental setup was used to determine the neutron capture cross sections of the tellurium isotopes in the energy range from 10 to 200 keV. The essential features of

this experiment are high efficiency and good energy resolution for the detection of capture gamma-rays as well as good time resolution and low sensitivity to sample scattered neutrons. Furthermore, the short primary flight path could be used to discriminate the background due to capture of sample scattered neutrons in the detector via time of flight. This unique combination allowed to determine the cross section ratio of the tellurium isotopes to the gold standard with an uncertainty of ~1 % , which represents an improvement of a factor of five compared to conventional techniques .

Accurate cross sections are essential for detailed studies of the element production in the s-process. For obtaining the stellar cross sections, the measured energy range was extended to 0 and to 600 keV by normalizing the cross section shape from literature to the present results. In this way, it was possible to determine the stellar values for the astrophysical applications with ~1 % uncertainty, too.

With these data it could be shown for the first time, that the classical s-process model describes the solar abundances of s-only nuclei at least locally very well, i.e. that the "local approximation" ($\langle\sigma\rangle N_s$= const for neighboring isotopes) is valid with an uncertainty of 1 %. It was also possible to derive limits for the p-process contributions of the s-only isotopes of tellurium. Preliminary calculations with a stellar model confirmed that the accurate data are essential for deciphering the information in the observed abundances completely, and to derive true constraints for the stellar environment by such analyses.

The present experiment starts a series of measurements for a systematic investigation of those branchings in the s-process path, that are characterized by two s-only nuclei, with the next examples being the pairs ^{148}Sm/^{150}Sm, ^{134}Ba/^{136}Ba, ^{128}Xe/^{130}Xe and ^{152}Gd/^{154}Gd. These results will allow to analyse known branchings with improved accuracy and to check for possible weak branchings presently presumed by model predictions. In this way, the $\langle\sigma\rangle N_s$ curve can be defined very accurately, and rather stringent predictions may be expected for the physical parameters during the s-process. These investigations, complemented by other new experiments, e.g. cross section studies for the radioactive branch point isotopes, will allow to use the s-process as a diagnostic tool for the stellar plasma, yielding improved insight in the mechanisms of helium shell burning in Red Giants.

IX. REFERENCES

[1] F. Käppeler, H. Beer, and K. Wisshak, Rep. Prog. Phys. **52**, 945 (1989).

[2] E. Anders and N. Grevesse, Geochim. Cosmochim. Acta **53**, 197 (1989).

[3] H. Holweger, in Les Elements et leurs Isotopes dans l'Univers, edited by A. Boury, N. Grevesse, and L. Remy-Battian, University of Liège, Liège (1979) p117.

[4] P. J. Patchett, 46th Annual Meeting of the Meteoritical Society, Mainz, Fed. Rep. of Germany, September 5-9 1983.

[5] H. Beer, G. Walter, R.L. Macklin, and P.J. Patchett, Phys. Rev. C **30**, 464 (1984).

[6] N. E. Holden, R.L. Martin, and I.L. Barnes, Pure Appl. Chem. **56**, 675 (1984).

[7] R.L. Macklin and R.R. Winters, Neutron capture of ^{122}Te, ^{123}Te, ^{124}Te, ^{125}Te, and ^{126}Te, report ORNL-6561 Oak Ridge National Lab. (1989).

[8] R.R. Winters, F. Käppeler, K. Wisshak, A. Mengoni, and G. Reffo, Ap. J. **300**, 41 (1986).

[9] K. Wisshak, K. Guber, F. Käppeler, J. Krisch, H. Müller, G. Rupp, and F. Voß, Nucl. Instr. Meth. **A292**, 595 (1990).

[10] K. Wisshak, F. Voß, F. Käppeler, and G. Reffo, Phys. Rev. **C42**, 1731 (1990).

[11] G. Winkler, Nucl. Instr. Meth. **A282**, 317 (1989)

[12] M. Mizumoto and M. Sugimoto, Nucl. Instr. Meth. **A282**, 324 (1989).

[13] Z.Y. Bao and F. Käppeler At. Data Nucl. Data Tables **36**, 411 (1987).

[14] G. Reffo, F. Fabbri, K. Wisshak, and F. Käppeler, Nucl. Sci. Eng. **80**, 630 (1982).

[15] K. Wisshak, F. Käppeler, and G. Schatz, Nucl. Instr. Meth. **221**, 385 (1984).

[16] F.H. Fröhner, SESH- A Fortran IV Code for Calculating the Self-Shielding and Multiple Scattering Effects for Neutron Cross Section Data Interpretation in the Unresolved Resonance Region, report GA-8380, Gulf General Atomic (1968).

[17] A. Gilbert and A.G.W. Cameron, Can. J. of Phys. **43**, 1446 (1965).

[18] R.M. Musaelyan and V.M. Skorkin, Bull. Acad. Sci. USSR **52**, 157 (1988).

[19] S.F. Mughabghab, M. Divadeenam, and N.E. Holden, Neutron Cross Sections, Vol.1, Part A (Academic Press, New York, 1981).

[20] C. Nordborg, H. Gruppelaar, and M. Salvatores, Proceedings of the International Conference on Nuclear Data for Science and Technology, Jülich, Germany, 13 - 17 may 1991, to be published.

[21] Y. Xia, Th. W. Gerstenhöfer, S. Jaag, F. Käppeler, and K. Wisshak, Phys. Rev. C submitted for publication.

[22] R.L. Macklin, private communication (1982)

[23] W. Ratynski and F. Käppeler, Phys. Rev. C **37**, 595 (1988).

[24] A.A. Bergman and S.A. Romanov, Sov. J. Nucl. Phys. **20**, 133 (1975).

[25] R.L. Macklin and J.H. Gibbons, Phys. Rev. **159**, 1007 (1967).

[26] H. Beer and F. Voß, Astrophys. J. submitted for publication.

[27] E.M. Burbidge, G.R. Burbidge, W.A.Fowler, and F. Hoyle, Rev. Mod. Phys. **29**, 547 (1957).

[28] P.A. Seeger, W.A. Fowler, and D.D. Clayton, Astrophys. J. Suppl. **11**, 121 (1965).

[29] D.D. Clayton and R.A. Ward, Astrophys. J. **193**, 397 (1974).

[30] F. Käppeler, R. Gallino, M. Busso, G. Picchio, and C.M. Raiteri, Astrophys. J. **354**, 630 (1990).

[31] R.A. Ward, M.J. Newmann, and D.D. Clayton, Astrophys. J. Suppl. **31**, 33 (1976).

[32] W. Schanz, Die Stellaren Neutroneneinfangquerschnitte von ^{120}Sn, ^{121}Sb, ^{123}Sb und ^{128}Te, Diploma Thesis University of Karlsruhe 1990, unpublished.

[33] H. Beer, G. Walter, and F. Käppeler, Astron. Astrophys. **211**, 245 (1989).

[34] J.A. Holmes, S.E. Woosley, W.A. Fowler, and B.A. Zimmerman, At. Data Nucl. Data Tables **18**, 305 (1976).

[35] K. Takahashi and K. Yokoi, At. Data Nucl. Data Tables **36**, 375 (1987).

[36] N. Klay, F. Käppeler, H. Beer, and G. Schatz, Phys. Rev. C in print.

[37] M. Rayet, N. Pranzos, and M. Arnould, Astron. Astrophys. **227**, 271 (1990).

[38] W.M. Howard, B.S. Meyer, and S.E. Woosley, Astrophys. J. **373**, L5 (1991).

[39] R. Gallino, M. Busso, G. Piccino, C.M. Raiteri, and A. Renzini, Astrophys. J. **334**, L45 (1988).

[40] R. Gallino, private communication (1990).

[41] S. Jaag, Diplom thesis, University of Karlsruhe (1990).

[42] K. Wisshak, W. Schanz, and F. Käppeler, in preparation.

X. ACKNOWLEDGMENTS

Many collegues from KfK helped us to bring this experiment to a successful end. In particular we would like to thank Ch. Adelhelm, E. Nold and G. Streib from the Institute of Material Research for their careful analyses of the oxygen and hydrogen content of the sample material. We also appreciated the spontaneous help of E. Gantner, H. Deutsch and J. Reinhardt from the Institute of Radiochemistry who determined the isotopic composition. The Van de Graaff crew, D. Roller, E.-P. Knaetsch and W. Seith did a great job in keeping the accelerator running at optimum conditions. Last not least, the continuous support of G. Rupp in optimizing the experimental setup is greatefully acknowledged.